

# Five More Massive Binaries in the Cygnus OB2 Association

Daniel C. Kiminki<sup>1</sup>, Henry A. Kobulnicky<sup>1</sup>, Ian Gilbert<sup>2</sup>, Sarah Bird<sup>3,4</sup>, Georgi Chunev<sup>5</sup>

## ABSTRACT

We present the orbital solutions for four OB spectroscopic binaries, MT145, GSC 03161-00815, 2MASS J20294666+4105083, and Schulte 73, and the partial orbital solution to the B spectroscopic binary, MT372, as part of an ongoing study to determine the distribution of orbital parameters for massive binaries in the Cygnus OB2 Association. MT145 is a new, single-lined, moderately eccentric ( $e = 0.291 \pm 0.009$ ) spectroscopic binary with period of  $25.140 \pm 0.008$  days. GSC 03161-00815 is a slightly eccentric ( $e = 0.10 \pm 0.01$ ), eclipsing, interacting and double-lined spectroscopic binary with a period of  $4.674 \pm 0.004$  days. 2MASS J20294666+4105083 is a moderately eccentric ( $e = 0.273 \pm 0.002$ ) double-lined spectroscopic binary with a period of  $2.884 \pm 0.001$  days. Schulte 73 is a slightly eccentric ( $e = 0.169 \pm 0.009$ ), double-lined spectroscopic binary with a period of  $17.28 \pm 0.03$  days and the first “twin” in our survey with a mass ratio of  $q = 0.99 \pm 0.02$ . MT372 is a single-lined, eclipsing system with a period of 2.228 days and low eccentricity ( $e \sim 0$ ). Of the now 18 known OB binaries in Cyg OB2, 14 have periods and mass ratios. Emerging evidence also shows that the distribution of  $\log(P)$  is flat and consistent with “Öpik’s Law”.

*Subject headings:* techniques: radial velocities — (stars:) binaries: general — (stars:) binaries: spectroscopic — (stars:) binaries: (*including multiple*) close — stars: early-type — stars: kinematics — surveys

## 1. Introduction

The study of massive binary systems in young clusters plays a key role in our understanding of how massive stars form. In addition to providing the binary fraction for massive

---

<sup>1</sup>Dept. of Physics & Astronomy, University of Wyoming, Laramie, WY 82070

<sup>2</sup>Dept. of Physics, Grove City College, Grove City, PA 16127

<sup>3</sup>Dept. of Physics & Astronomy, University of Turku, Turku, Finland

<sup>4</sup>Tuorla Observatory, Piikkiö, Finland

<sup>5</sup>Dept. of Computer Science, Indiana University, Bloomington, IN 47405

stars, massive binary systems provide information about their formation environment in the form of quasi-preserved parameters such as eccentricity, separation, period, and angular momentum (in the form of rotational velocities; Larson 2001). In addition, an initial mass function (IMF) composed of the secondary component masses can indicate whether the companions are randomly drawn from a Salpeter (1955) (or equivalent field star) IMF or not. This can tell us whether the binary systems may have randomly formed by way of gravitational capture after the formation process, or preferentially paired through a more complicated formation process such as competitive accretion (Bonnell et al. 1998).

Cyg OB2 provides one of the best regions for indirectly examining the formation of massive stars as it houses  $\sim 60$ – $70$  O-type stars (Negueruela et al. 2008), including an O3If (Schulte 7; Walborn & Howarth 2000) and an O4If (Schulte 22; Comerón & Pasquali 2007), and possibly more than 2000 B stars (Knödlseher 2000). Kiminki et al. (2008) presented six new spectroscopic binary systems and summarized the then-known 11 OB binary systems in Cyg OB2. Between then and this work, three additional OB binary systems have been uncovered, including Schulte 9 (Nazé et al. 2008), 2MASS J20302730+4113253 (Stroud et al. 2009, submitted), and GSC 03161-00815 (Otero 2008a; Hanson 2003). Six of the total 14 systems, MT421, MT429, MT696, Schulte 3, Schulte 5, and GSC 03161-00815 are identified as eclipsing binaries (where notation for the first five are from Massey & Thompson 1991 and Schulte 1956). Two of the 14 systems, MT059 and MT258, are single-lined spectroscopic binaries (SB1s), and eight of the 14, MT252, MT696, MT720, MT771, Schulte 3, Schulte 8a, Schulte 9, and 2MASS J20302730+4113253, are double-lined spectroscopic binaries (SB2s). In part three of this ongoing study, we add to the 14 and present the newly uncovered spectroscopic binaries, MT145 (SB1), 2MASS J20294666+4105083 (listed as a candidate SB2 in Hanson 2003), Schulte 73 (SB2), and MT372 (SB1). We also present the first spectroscopic solution to the eclipsing system, GSC 03161-00815 (SB2). For simplicity, we will use Comerón et al. (2002) notation for GSC 03161-00815, 2MASS J20294666+4105083, and 2MASS J20302730+4113253 (A36, A45, and B17 respectively). These new systems bring the total number of OB binaries in Cyg OB2 to 18, constituting one of the highest numbers of massive binary solutions of any open cluster.

Section 2 of this work provides observational details of the new spectroscopic datasets. Section 3 discusses the measurement of radial velocities, the search for periods in the radial velocity data, and the determination of orbital elements via radial velocity curve fitting. Section 4 discusses the orbital solutions to the SB1, MT145, and the SB2s, A36, A45, and Schulte 73 (Cyg OB2 No. 73). Section 5 presents the partial solution to the SB1, MT372. Finally, Section 6 summarizes the results of the survey to date, including the total number of OB binaries uncovered in the Cyg OB2 core region, the total number of O star binary solutions, and the emerging distribution of orbital periods.

## 2. Observations

Kiminki et al. (2007) & Kiminki et al. (2008) (Papers I & II) detail the observations of this survey through 2007 September. We have obtained additional datasets with the WIRO-Longslit spectrograph<sup>1</sup> on the Wyoming Infrared Observatory (WIRO) 2.3 m telescope and the Hydra spectrograph on the WIYN<sup>2</sup> 3.5 m telescope. Table 1 lists the observing runs at each facility, the corresponding spectral coverages, and mean spectral resolutions.

Observations at WIYN took place over six nights on 2008 June 10–15. We used the Hydra spectrograph with the Red camera, 2'' blue fibers, and the 1200 l mm<sup>-1</sup> grating in second order to obtain four 1500 s exposures in each of two fiber configurations yielding a maximum signal-to-noise ratio (SNR) of 80:1 for the brightest stars. The spectral coverage was 3820–4500 Å at a mean resolution of  $R \sim 4500$ . Copper-Argon lamps were used between each exposure to calibrate the spectra to an RMS of 0.03 Å (2 km s<sup>-1</sup> at 4500 Å), and the typical resolution was 1.0 Å FWHM at 3900 Å and 0.82 Å FWHM at 4400 Å. Spectra were Doppler corrected to the heliocentric frame and checked against the radial velocity standards HD131156 (G8V), HD146233(G2V), HD161096(K2III), HD161797(G5IV), and HD171391(G8III) from Stefanik et al. (1999) before comparison to previous datasets.

Observations using the WIRO-Longslit spectrograph with the 1800 l mm<sup>-1</sup> grating in first order took place over 37 nights between 2007 October 23 and 2008 September 19 to examine the H $\alpha$ , He I, and He II absorption lines in suspected SB2s. Exposure times varied from 600 s to 4500 s (in multiples of 600–900 s) depending on weather conditions and yielded a maximum SNR of 200:1 for the brightest stars. The spectral coverages were 5500–6750 Å (2007 October 23 through 2007 November 5) and 5250–6750 Å (2008 June 23 through 2008 September 19). Copper-Argon lamp exposures were taken after each star exposure to wavelength calibrate the spectra to an rms of 0.03 Å (1.4 km s<sup>-1</sup> at 6400 Å). The typical spectral resolution was 1.5 Å FWHM across the chip. Spectra were Doppler corrected to the heliocentric frame and checked against the same radial velocity standards taken during the 2008 June observations at WIYN before comparison to previous datasets. In addition, we also cross-correlated the WIRO-Longslit spectra with a composite interstellar line spectrum to look for systematic relative radial velocity shifts. The interstellar line spectrum was created by extracting the interstellar lines present in the 2008 spectra of A36, Doppler shifting them to the same velocity and combining them. Interstellar lines and diffuse

---

<sup>1</sup>The WIRO-Longslit spectrograph was constructed by M. J. Pierce and A. Monson at the University of Wyoming. Instrument information can be found at [http://physics.uwyo.edu/~amonson/wiro/long\\_slit.html](http://physics.uwyo.edu/~amonson/wiro/long_slit.html)

<sup>2</sup>The WIYN Observatory is a joint facility of the University of Wisconsin, Indiana University, Yale University, and the National Optical Astronomy Observatory

interstellar bands were identified with Herbig (1975), Herbig & Leka (1991), Morton (1991), and Galazutdinov et al. (2000). Relative velocity shifts were generally less than  $6 \text{ km s}^{-1}$ . Observations with relative shifts larger than  $6 \text{ km s}^{-1}$  were corrected to the average absolute radial velocity offset before computing orbital solutions. All new datasets were reduced using standard IRAF reduction routines as outlined in Paper I.

### 3. Data Analysis and Orbital Solutions

#### 3.1. Measuring Radial Velocities and Estimating Errors

We obtained radial velocities,  $V_r$ , for the single-lined system, MT145 via the IRAF cross-correlation task XCSAO in the RVSAO package (Kurtz et al. 1991), using a model stellar atmosphere (Lanz & Hubeny 2003, TLUSTY) of the appropriate effective temperature and gravity as discussed in Paper I. Errors within the XCSAO task are calculated using,

$$\sigma_v = \frac{3w}{8(1+r)}. \quad (1)$$

where  $w$  is the FWHM of the correlation peak and  $r$  is the ratio of the correlation peak height to the amplitude of antisymmetric noise (Kurtz et al. 1991).

To obtain rough  $V_r$  measurements for the double-lined systems, A36, A45, and Schulte 73, we deblended the He I  $\lambda\lambda 4471, 5876$  (A36 & Schulte 73) or H $\alpha$  (A45 & MT372) lines by fitting simultaneous Gaussian profiles (at fixed Gaussian widths) with the SPLOT routine in IRAF. We repeated this method 10 times while varying the baseline region used to define the continuum each time. We then used the mean of each component’s list of Gaussian centers to compute the velocity. Utilizing this method, a number of factors contribute to the radial velocity uncertainty. These factors include, but are not limited to the errors associated with Gaussian profile fitting, wavelength calibrations, emission present in the line cores, and lower signal-to-noise of the less-luminous component’s spectral profiles (especially while in a partially or wholly blended state). We estimated the contribution of the Gaussian profile fitting uncertainty by adopting the rms of each component’s list of Gaussian centers. Unfortunately, this only produces a lower limit on the uncertainty because the initial Gaussian width estimates also affect the center measurements. For the total one-sigma uncertainties, we adopted these rms values combined in quadrature with the typical error in the wavelength calibration ( $1.4 \text{ km s}^{-1}$  for WIRO and  $2 \text{ km s}^{-1}$  for WIYN) and the typical rms observed in the list of velocities obtained from the correlation with the interstellar line template. The total error given for each system reflects a lower limit as we cannot characterize uncertainty

contributions from emission present in the line cores (e.g., A36) or the lower SNR of the secondary spectral features (e.g., A45).

### 3.2. Determining Orbital Solutions

We used the method outlined in McSwain (2003) to determine the orbital parameters of each system. We obtained an estimate of the orbital period through an IDL<sup>3</sup> program written by A. W. Fullerton which makes use of the discrete Fourier transform and CLEAN deconvolution algorithm of Roberts et al. (1987). The strongest peaks in the power spectrum of each star were examined by folding the data at the corresponding period and inspecting the  $V_r$  curve visually. Orbital elements were then procured by using the best period as an initial estimate in the nonlinear, least-squares curve fitting program of Morbey & Brosterhus (1974). The best solutions were attained by manually varying the initial guesses of key orbital parameters until a minimum in the *rms* of the fit was found. Weights for each point were assigned as the inverse of the  $1\sigma$   $V_r$  error.

While it is not uncommon to quote orbital period errors to one ten thousandth of a day (e.g., Williams et al. 2008; Penny et al. 2008; Linder et al. 2007; McSwain 2007; Hillwig et al. 2006), we performed two additional tests to evaluate the appropriateness of the orbital period uncertainties for each system. In the first test, we explored the confidence range for each orbital parameter by fitting the radial velocity data 1000 times, with the orbital parameters as free variables, while adding Gaussian noise to the data. The noise added to each data point was characterized by the one-sigma uncertainty. We compared the resultant rms deviations to the single-fit error estimates for each orbital parameter. The result of this test suggested that the majority of the single-fit parameter uncertainties were reasonable, as the Monte Carlo test routinely produced similar uncertainties. The disadvantage to this test, however, is that we could not examine each fit to see if it was reasonable (i.e., whether the newly folded radial velocities had a reasonable rms). Therefore, with the error in the period strictly in mind, we ran the orbital fitting procedure 50–100 times while incrementing the period by the single-fit error estimate and monitored how the rms changed. The result of this test suggests that we, at most, underestimate the orbital period errors by a factor of 10. With this in mind, the errors for the orbital period throughout this work have been increased by a factor of ten.

The complete list of orbital elements for each binary system appears in Table 2. Listed within the table are the period in days ( $P$ ), eccentricity of the orbit ( $e$ ), longitude of pe-

---

<sup>3</sup>The Interactive Data Language (IDL) software is provided by ITT Visual Information Solutions.

riastron in degrees ( $\omega$ ), systemic radial velocity ( $\gamma$ ), epoch of periastron ( $T_0$ ), primary and secondary semi-amplitudes ( $K_1$  &  $K_2$ ), adopted or calculated minimum primary and secondary masses in solar masses ( $M_1$  &  $M_2$ ), primary and secondary mass functions in solar masses ( $f(m)_1$  &  $f(m)_2$ ), spectral classifications from this survey ( $S.C._1$  &  $S.C._2$ ), the minimum primary and secondary semi-major axes in solar radii ( $a_1 \sin i$  &  $a_2 \sin i$ ), and finally, the rms of the fits ( $rms_1$  &  $rms_2$ ).

### 3.3. A Note on Systemic Velocities

Systemic radial velocities are known to vary depending on which lines are used to measure the radial velocity. This is especially evident with massive stars and evolved stars where the stellar atmosphere velocity gradient may be higher (see Linder et al. 2007 for examples with a few well-studied O binaries). To minimize such discrepancies, radial velocities are normally averaged over many lines. In the case of MT145, where we obtain radial velocities by cross correlation over many lines, this is not an issue. However, in the case of the remaining 4 systems, we only have 1–2 lines (He I  $\lambda\lambda$  5876, 6678 or H $\alpha$ ) available for radial velocity measurement in the majority of spectra. This places an added uncertainty on the systemic velocity and semi-amplitudes measured for A36, A45, Schulte 73, and MT372. In the simplest case, these effects may cause a systematic blueshift to the systemic velocity (such as the case with a non-eclipsing system with equal and symmetric stellar winds). Eclipses, uneven stellar winds, and uneven surface temperatures complicate the matter, and these effects can affect the components unequally, producing systemic radial velocities that vary from primary to secondary. We see this effect in two of our systems, A45 and Schulte 73. The component orbital solutions produce two different systemic velocities. For both of these systems, we adopted the mean of the two values as the systemic velocity of the system for Table 2.

## 4. Orbital Solutions for MT145, A36, A45, & Schulte 73

### 4.1. The SB1 MT145

We observed MT145 a total of 54 times, including 6 at Lick, 2 at Keck, 12 at WIYN, and 34 at WIRO. Excluding two low-SNR spectra from Lick and one from WIRO, a total of 51 spectra were of sufficient SNR to obtain the solution for this O9III star. The strongest signal in the CLEANed power spectrum corresponds to a period of 25.12 days. An alias at 20 days is also present. However, the 20 day period produced a folded  $V_r$  curve having a much larger rms than the 25.12 day period. The best-fitting orbital solution and  $V_r$  curve for MT145 is

shown in Figure 1, corresponding to a period of  $P = 25.140 \pm 0.008$  days with an eccentricity of  $e = 0.291 \pm 0.009$  and solution  $rms = 8.9 \text{ km s}^{-1}$ . With this period, a semi-amplitude of  $K_1 = 48.9 \pm 0.7 \text{ km s}^{-1}$ , and an assumed primary mass of  $M_1 = 22.6 \pm 0.5 M_\odot$  (Martins et al. 2005), we estimate a minimum secondary mass of  $M_2 = 6.0 \pm 0.1 M_\odot$ , corresponding to a mid B star (interpolated from Drilling & Landolt 2000). This yields a mass ratio lower limit of  $q = M_2/M_1 \gtrsim 0.27 \pm 0.01$ . To constrain the mass ratio upper limit, we examined the spectra taken while the system was near quadrature for evidence of line-doubling or asymmetries originating from the secondary. Neither is present in any of the spectra. Given SNR ratios of up to 150:1 for these spectra, we would expect to see evidence of the secondary star’s spectral features at velocity separations of  $(1 + 1/q)K_1$  if the component luminosity ratio is larger than  $L_2/L_1 \simeq 0.2$ . This maximum luminosity ratio is determined by combining synthetic spectra at various luminosity ratios and line separations. The absence of secondary spectral features therefore conservatively limits the luminosity ratio to  $L_2/L_1 \lesssim 0.2$  and implies a secondary less luminous than a B1V (interpolated from Drilling & Landolt 2000). We thus constrain the mass of the secondary to  $6.0 \pm 0.1 M_\odot < M_2 \lesssim 13.8 \pm 0.6 M_\odot$  and the mass ratio to  $0.26 \lesssim q \lesssim 0.63$  (where the range in mass ratio incorporates both observational and inclination uncertainties). These limits loosely require  $i \gtrsim 31^\circ$  given the uncertainty in O star masses (Massey et al. 2005). Additionally, the solution produces a minimum primary semi-major axis of  $a_1 \sin i = 23.2 \pm 0.3 R_\odot$  and a longitude of periastron of  $\omega = 158.3^\circ \pm 0.6^\circ$

The ephemerides for MT145 and MT372 are listed in Table 3 and include the date ( $HJD - 2,400,000$ ), phase ( $\phi$ ), measured radial velocity ( $V_r$ ), cross-correlation  $1\sigma$  error ( $1\sigma \text{ err}$ ), and the observed minus calculated velocity ( $O - C$ ).

## 4.2. The SB2 A36

A36 is originally introduced as a probable massive member of Cyg OB2 in Comerón et al. (2002) and listed as a possible binary based on the asymmetry in the absorption lines of a high SNR spectrum in Hanson (2003, Figure 1). Otero (2008a) provided a partial photometric solution to this system and listed it as an eclipsing binary of the Algol type with evidence of an O’Connell effect (a light curve having unequal out-of-eclipse maxima; Milone 1968). We provide the first spectroscopic solution to this double-lined system.

We observed A36 a total of 23 times between 2007 October and 2008 August, including 5 times with Hydra at WIYN and 18 times with the WIRO-Longslit spectrograph. With the 19 higher SNR spectra we obtained a period estimate of 4.680 days from the CLEANed power spectrum with no aliases. From this estimate we obtained the solution for the secondary ( $rms=10.0 \text{ km s}^{-1}$ ) shown in Figure 2 with a period of  $P = 4.674 \pm 0.004$  and relatively

low eccentricity of  $e = 0.10 \pm 0.01$ . The period, eccentricity, epoch of periastron, and systemic velocity were applied as fixed parameters to obtain the solution for the primary (rms=29.3 km s<sup>-1</sup>). The filled symbols correspond to the primary  $V_r$  measurements and the open symbols correspond to the secondary  $V_r$  measurements. The combined solutions provide minimum semi-amplitudes of  $K_1 = 169 \pm 9$  km s<sup>-1</sup> and  $K_2 = 243 \pm 2$  km s<sup>-1</sup> for the primary and secondary, respectively, and produce semi-major axes of  $a_1 \sin i = 15.6 \pm 0.8 R_\odot$  and  $a_2 \sin i = 22.345 \pm 0.003 R_\odot$ . The computed lower limit masses of  $M_1 \sin^3 i = 19.8 \pm 0.9 M_\odot$  and  $M_2 \sin^3 i = 13.8 \pm 0.9 M_\odot$  yield a mass ratio of  $q = 0.70 \pm 0.06$ . Table 4 provides the ephemerides for A36, A45, and Schulte 73, listing the date (HJD–2,400,000), phase ( $\phi$ ), measured radial velocities ( $V_{r1}$  and  $V_{r2}$ ), and observed minus calculated velocities ( $O_1 - C_1$  and  $O_2 - C_2$ ). Error estimates are shown in parentheses.

Based on two of the spectra obtained during the 2008 WIYN run, we tentatively classify the components of A36 as a B0Ib and B0III for primary and secondary respectively. The exposures obtained on 2008 June 10 & 15 show the components at nearly the same phase and in quadrature. Additionally, the light curve shown in Otero (2008a), tells us that the temperatures of the components are similar, and the double-lined nature of the spectra tell us that the luminosities are similar. We can therefore conclude from the 2008 June 10 spectrum shown first from the top in Figure 4 that the spectral types of the components are similar with subtle differences, such as stronger Si IV  $\lambda\lambda$  4089, 4116 and weaker He I  $\lambda\lambda$  4026, 4121, 4387, 4471 for the primary. Both primary and secondary have no Mg II  $\lambda$  4481 (confirmed in Figure 1 in Hanson 2003), moderately strong Si IV  $\lambda\lambda$  4089, 4116, strong He I  $\lambda\lambda$  4026, 4471, weak He I  $\lambda\lambda$  4121, 4387, and strong C III  $\lambda$  4070. After smoothing the WIYN spectra to approximately the resolution of the spectra in the Walborn & Fitzpatrick (1990) digital atlas, we combined a B0Ib (HD164402) spectrum with a B0III (HD48434) spectrum at the appropriate radial velocities to make a comparison. The resulting combined spectrum (second from top) is also shown in Figure 4 along with the 2001 September 8 spectrum of Schulte 73 (second from bottom) obtained at WIYN and the associated composite spectrum for Schulte 73 (bottom). Intrinsic He I, He II, C III, Si IV, Mg II, and hydrogen absorption are labeled. The composite spectrum is not an exact match to A36 (note that Si IV 4089 is stronger than that of the primary). However, the mass ratio obtained from Drilling & Landolt (2000) for a B0Ib primary and B0III secondary is  $q = 0.8$  and agrees with our calculated mass ratio of  $q = 0.70 \pm 0.06$ .

An apparent weakening of the primary’s He I lines between phases 0.218 and 0.609, seen in panels 1 and 3 of the time series presented in Figure 3, at least partially explains the large residuals at these epochs and may originate from a Struve-Sahade effect (Linder et al. 2007). This apparent weakening also coincides with an absence of well-defined absorption profiles in H $\alpha$  (panel 2 of Figure 3) between secondary and primary eclipse. These spectral phenomena

coupled with the continuous variation of the light curve presented in Otero (2008a) associated with Algol eclipsing systems, an O’Connell effect (which is generally associated with contact or near contact systems; Liu & Yang 2003) and a seemingly close separation between components ( $a_{\text{sin}i} \sim 28 R_{\odot}$ ), implies that A36 is either a contact or near-contact system. In the very least, it is likely that one or both components are filling their Roche lobes. Because A36 is composed of B stars, one may question whether this is a Be binary. The system does not hold the standard qualifications for a Be binary however, as the mass ratio is much greater than 0.1 and the primary is evolved (Harmanec 2002). Conti & Leep (1974, Figure 3) also show that hot supergiants can have hydrogen emission that very closely resembles the double-peaked hydrogen emission seen in Be stars.

Is A36 a member of Cyg OB2? Hanson (2003) places doubt on its status as a member of the cluster based on its disagreement with the 2 Myr isochrone and evolutionary tracks best fit for Cyg OB2 stars. With a systemic velocity offset  $-36 \text{ km s}^{-1}$  from the mean systemic velocity for cluster stars ( $-10.3 \text{ km s}^{-1}$ ; Paper I), A36 is likely either a runaway binary system or a background system masquerading as a member of Cyg OB2. McSwain (2007) found observational evidence for several runaway binary systems, but concluded that they are rare. These systems can be produced by an asymmetric supernova of one of the components (producing an SB1) or by dynamic interactions within a dense cluster. With a stellar density of  $\rho_0 = 40 - 150 M_{\odot}$  (Knödlseeder 2000) it is certainly possible for A36 to have originated this way, but not probable. However, as a background object, A36’s systemic velocity inferred from a Galactic rotation curve, would place it at a distance of 6.6 kpc, an interarm region where OB stars are unlikely to form. Therefore, without a proper motion to trace its trajectory, or until a complete solution is computed for the photometric and spectroscopic solutions for this star, the status of A36’s membership will remain uncertain.

### 4.3. The SB2 A45

We obtained 24 observations from 2007 October through 2008 September on this double-lined system. Hanson (2003) classified this star a B0.5V, but, as with A36, she also suggests it may be an SB2 based on a high SNR spectrum (see Figure 1 in Hanson 2003). We present the first confirmation of the binary nature of A45 with a spectroscopic solution to this system.

Of the 24 observations, we used 21 to obtain rough  $V_r$  measurements with the  $H\alpha$   $\lambda 6562.80$  line. We did not use the He I  $\lambda\lambda 5875.75, 6678.15$  lines owing to either the weaker He I absorption of the secondary or low SNR of the spectra near He I  $\lambda 5876$ . The 18 measurements produced a CLEANed power spectrum with a period estimate of 2.885 days and aliases

of 2 days and 1.55 days. The latter is a  $1 - \nu$  alias (where  $\nu$  is the signal frequency per day). Neither alias produced a folded  $V_r$  curve with as low of an rms as 2.885 days. The best solution for the primary results in a period of  $P = 2.884 \pm 0.001$  and eccentricity of  $e = 0.273 \pm 0.002$ . The period, eccentricity, and epoch of periastron were applied as fixed parameters to obtain the solution for the secondary. The rms of  $47 \text{ km s}^{-1}$  indicates there is room for improvement in the secondary’s solution and also explains the high uncertainty on the calculated masses,  $M_1 \sin^3 i = 12 \pm 1 M_\odot$  and  $M_2 \sin^3 i = 5.3 \pm 0.5 M_\odot$  ( $q = 0.6 \pm 0.1$ ). With minimum semi-amplitudes of  $K_1 = 126.1 \pm 0.3 \text{ km s}^{-1}$  and  $K_2 = 273 \pm 17 \text{ km s}^{-1}$  for the primary and secondary respectively, the solution also produces minimum semi-major axes of  $a_1 \sin i = 6.91 \pm 0.02 R_\odot$  and  $a_2 \sin i = 14.96 \pm 0.01 R_\odot$  and a systemic velocity of  $\gamma = 5 \pm 1 \text{ km s}^{-1}$ .

We have limited information for classification of the components of A45 owing to the limited spectral coverage of the WIRO-Longslit datasets ( $\sim 5300\text{--}6700 \text{ \AA}$ ). No attempt to obtain exposures of this system was made during the 2008 WIYN run because of the system’s angular separation from the rest of the sample. Examination of the existing spectral coverage and the spectrum in Figure 1 of Hanson (2003) suggests that her classification is more or less accurate in the sense that both components appear to be early B stars. There is no evidence of He II in either component, He I is moderately strong, Mg II is weak, and there appears to be no Si IV. An absence of the numerous additional metal lines, such as O II, C II, C III, and N II seen in evolved B stars suggests that neither component is very evolved and both are likely still dwarves. Additionally, a double-lined system with a mass ratio of  $q = 0.6 \pm 0.1$  restricts the secondary component to within one or two temperature classes of the primary component. Therefore, we adopt the classification of B0.5V for the primary and B2V?–B3V? for the secondary component based on the aforementioned line strengths and mass ratio.

Is A45 a member of Cyg OB2? Although A45 has the largest angular separation from the core of Cyg OB2, the systemic velocity agrees with the mean systemic velocity of cluster members and the system does show the same diffuse interstellar band features characteristic of Cyg OB2 stars. Additionally, though the combined luminosity and temperature of the system disagrees slightly with its predicted placement on the H-R diagram presented for Cyg OB2 stars in Figure 12 in Hanson (2003), individual component luminosities and temperatures shift A45’s position down on the diagram and into better agreement with other Cyg OB2 members.

#### 4.4. The SB2 Schulte 73

Schulte 73 is included in our original sample but excluded from Paper I owing to the less than 3 observations then obtained. Spectra taken during the 2008 June WIYN run, however, revealed the double-lined nature of this star, and re-examination of the 2001 September 8 spectrum confirmed it. The successive 2008 WIRO runs cemented its status as a double-lined spectroscopic binary with a period of  $\sim 17.3$  days and a mass ratio nearly equal to unity. The solution computed for Schulte 73 utilized 27 of the 36 spectra obtained. Seven spectra from WIYN in 2008 June were excluded for low SNR owing possibly to a fiber position discrepancy. Two WIRO spectra (2008 July 26 & 27) were excluded because of the extremely blended state of the components.

For the 27 higher SNR spectra, the initial period estimate from the CLEANed power spectrum is  $\sim 16.6$  days with an alias at  $\sim 66$  days. We dismiss the alias on the basis that progression of the absorption lines from a blended to debled state is observed over approximately 4–5 nights. The best orbital solutions yield a period of  $P = 17.28 \pm 0.03$  days for both components. The exact period, eccentricity, and date of periastron are held constant for the primary in order to facilitate a matching solution with the secondary. Coincidentally, this also provides a better-fitting solution to the primary  $V_r$  curve. We attribute the larger error on the period (a magnitude higher than the other three systems) to the smaller number of velocity measurements obtained around apastron ( $\phi \simeq 0.3 - 0.6$ ). The solutions and corresponding  $V_r$  curves for Schulte 73 are shown in Figure 6. The filled and open symbols correspond to the primary and secondary  $V_r$  measurements respectively. The errant WIYN measurements in the primary solution (triangles) reflect the lower SNR of the 2008 June dataset and the error in the computed period. With an eccentricity of  $e = 0.169 \pm 0.009$  and semi-amplitudes of  $K_1 = 117 \pm 2 \text{ km s}^{-1}$  and  $K_2 = 117.9 \pm 0.8 \text{ km s}^{-1}$  the solutions produce masses of  $M_1 \sin^3 i = 11.2 \pm 0.2 M_\odot$  and  $M_2 \sin^3 i = 11.1 \pm 0.2 M_\odot$ . This results in a mass ratio of  $q = 0.99 \pm 0.02$  and our first confirmed “twin” in the cluster. The resulting semi-major axes are  $a_1 \sin i = 39.4 \pm 0.5 R_\odot$  and  $a_2 \sin i = 39.675 \pm 0.004 R_\odot$  (i.e., a separation of  $a \sin i = 79.075 \pm 0.5 R_\odot$ ), and the calculated systemic velocity is  $\gamma = -11 \pm 2 \text{ km s}^{-1}$ .

Massey & Thompson (1991) classify this star as an O8V. The components each show spectral signatures indicative of a later O type star, namely moderate to weak He II and stronger He I absorption. The primary classification criteria for later O type stars is He II  $\lambda 4542$ :He I  $\lambda 4387$  and He II  $\lambda 4200$ :He I  $\lambda 4144$  (Walborn & Fitzpatrick 1990). The  $\lambda 4200$ :He I  $\lambda 4144$  ratio (also sensitive to luminosity class) and a visual comparison with the 2001 September 8 spectrum from WIYN seen second from bottom in Figure 4 agree best with an O8III spectral type for both components. The Schulte 73 spectrum has been smoothed to approximately the resolution of the Walborn & Fitzpatrick (1990) digital atlas. However, without a

separation of the spectral components (e.g., tomographic separation), there is uncertainty in this assessment. The components also closely match an O7III and O9III spectral type. The very weak He I  $\lambda 4144$  however, precludes a later temperature class. The O8III (HD36861) and O8III composite spectrum is shown at the bottom of Figure 4. We also tried various combinations of an O8V, O8III and O8II. These did not fit the data as well and left larger residuals when subtracted from the Schulte 73 spectrum.

## 5. Partial Solution to the SB1 MT372

MT372 is a single-lined spectroscopic binary and an eclipsing system, likely of Algol type, with a period of  $P \sim 2.228$  days. With a visual magnitude of nearly 15, only 5 of our 21 spectroscopic observations of this B0V star are of sufficient SNR for meaningful analysis. Therefore, to assist in the period determination, we acquired the available photometric data for MT372 from the public data release of the Northern Sky Variability Survey (Wozniak et al. 2004), and ran it through our CLEAN IDL program to search for a period. While excluding points with errors greater than 0.2 magnitudes, we computed a period of  $P = 1.114$  days from the power spectrum. In the case that the light curve exhibits only a primary eclipse, the peak in the power spectrum corresponds to the real period of the system. In the case that the light curve exhibits both a primary and secondary eclipse, the peak corresponds to half the real period. We adopt the latter case because a period of 1.114 days produces an radial velocity orbital solution with an unacceptably large rms (where the radial velocities are determined from the  $H\alpha$  line in a similar manner to the SB2s). A period of  $P = 2.228$  produces the folded  $V_r$  curve and solution shown in Figure 7. In order to obtain this solution, we fixed the period and the eccentricity ( $e = 0$ ). Allowing the period and/or eccentricity to vary did not produce a viable solution, and we did not expect it would because of the very small number of radial velocities to work with. Although very noisy, this new period also produced a light curve with two eclipses (primary and secondary; seen in Figure 8) as opposed to the single primary eclipse present at a folding of 1.114 days. It should be noted, that the period of 1.114 days also produced a single eclipse that was asymmetric, suggesting that the time between primary and secondary eclipses and secondary and primary eclipses is not equal (i.e., the system seems to have a slight eccentricity). The orbital solution shown in Figure 7, also produces a semi-amplitude of  $K_1 = 75 \pm 20 \text{ km s}^{-1}$ , and a semi-major axis of  $a_1 = 3.4 \pm 0.9$ .

As this system has little evidence for a double-lined nature, we stay with the previous spectral classification of this star, B0V. A small change in velocity width seems to be visible in  $H\alpha$  in Figure 9 (panel 2), but the SNR of the spectra (especially evident with the He I

5876 and 6678 lines shown in panels 1 & 3 of Figure 9) makes it difficult to produce an accurate determination. The minimum secondary mass determined from the solution is  $M_2 = 3.5 \pm 0.9$ , assuming a primary of  $M_1 = 17.5$  (Drilling & Landolt 2000). Interpolating from Drilling & Landolt (2000) and reasonably assuming that the secondary is also unevolved, this results in a minimum spectral class of B8V. However, a B8V is unlikely to be the companion spectral class as it has too low of an effective temperature to produce the light curve in Figure 8. With a primary effective temperature of  $T_{eff} = 30,000$  K (Drilling & Landolt 2000) and a period of  $P = 2.228$  days, a B2V at a relatively high inclination ( $\sim 75$  degrees) would have the correct effective temperature and stellar radius to produce a light curve that resembles the one for MT372. However, given a B2V companion and a mass ratio of  $q \sim 0.6$ , the computed semi-major axis at approximately 75 degrees is not large enough to fully separate the two components. This may be explained by returning to the possible velocity width variation present in the H $\alpha$  lines. If indeed there is a small amount of blending of component profiles present, then fitting a single Gaussian profile to the blended H $\alpha$  line will systematically produce a smaller primary velocity amplitude and, in turn, smaller semi-amplitude and semi-major axis. We thus report the listed primary velocity semi-amplitude as a lower limit.

## 6. Summary of Current Survey Results

In this work, the third part of our ongoing survey to determine the distribution of binary orbital parameters in the Cyg OB2 association, we presented three new binary systems (MT145, Schulte 73, & MT372) and confirmed the binary status of one massive binary candidate (A45). We also provided the first spectroscopic orbital solution to the eclipsing binary, A36 and a partial solution to the eclipsing, single-lined system, MT372. While MT145, Schulte 73, A45, and MT372 are likely members of the cluster based on their systemic velocities (deviating by only  $\sim 0.6$ – $15$  km s $^{-1}$  from the cluster mean of  $-10.3$  km s $^{-1}$  obtained in Paper I and well within the Association’s radial velocity dispersion) the status of A36, with a systemic velocity of  $\gamma = -47$  km s $^{-1}$ , remains uncertain. The system could be a runaway binary or a background object (though both do not seem very probable). However, if we do include A36, the current total for OB binaries in Cyg OB2 is now 18. Of these 18, 14 have period and mass ratio estimates. In addition, with six partial spectroscopic solutions, eight full spectroscopic solutions, three partial photometric solutions, and four full photometric solutions, Cyg OB2 is on a track to become the cluster with the highest number of OB binary solutions. At seven it currently ties NGC 6231 (Sana et al. 2008) for the highest number of full O-star binary solutions. The locations of all 18 systems are shown in Figure 10. No evidence of grouping is apparent.

Table 5 lists several key parameters for all 18 systems, including the star designation, photometric and/or spectroscopic binary type (*Type*), spectral classifications (*S.C.*), period (*P*), mass ratio when available (*q*), and literature references (*Ref*). With the exception of Schulte 9 ( $P = 2.355$  years), periods for all systems are less than 25.2 days, with a mean of 9.6 days. Eleven systems have a period less than 5 days.

The 17 systems with periods less than 25.2 days also appear to obey Öpik’s Law (Öpik 1924), which states that the distribution of  $\log(P)$  is flat. To avoid histogram binning selection effects, we choose to show the normalized cumulative distribution of the logarithm of the periods (open diamonds) in Figure 11. The flat relation of Öpik’s law translates to a linear relation in a cumulative distribution. For comparison purposes, we also include the normalized cumulative distributions of O binaries in NGC 6231 (Sana et al. 2008, solid triangles) and the 54 OB binaries from the 9th Spectroscopic Binary catalog (Pourbaix et al. 2004, asterisks). All 3 cumulative distributions contain systems with periods less than 25.2 days and were normalized at a period of 8.9 days. To test the linearity of the Cyg OB2 distribution, we computed its linear Pearson correlation coefficient. The distribution yields a coefficient of  $r = 0.97$  (where  $r = 1$  is a perfectly linear relation). The linearity is illustrated by the best fit line (solid line) in Figure 11. The dashed line in the figure represents a perfect Öpik distribution (i.e., a perfectly flat distribution within the range of periods in Cyg OB2). A two sided Kolmogorov-Smirnov ( $K - S$ ) test between the Öpik and Cyg OB2 distributions gives a 38% probability that both were drawn from the same parent distribution.  $K - S$  tests between Cyg OB2 and NGC 6231 on the one hand and Cyg OB2 and the 9th Spectroscopic Binary catalog ( $P < 26$  days) on the other, yield 91% and 62% probabilities of being drawn from the same parent distribution, respectively. Interestingly, the cumulative distributions of Cyg OB2 and NGC 6231 have a high correlation and are very similar in appearance, including an upturn near  $\log(P) \sim 0.4 - 0.9$ . One wonders if this upturn is a true deviation from a linear relation (i.e., a preference for periods around 5 days), just a coincidence related to small number statistics, or observational bias. Though the latter case is a possible explanation for the upturn in NGC 6231, we do not believe this is the case with Cyg OB2 because several of the systems with periods around 5 days come from other programs with different observational cadences (e.g., MT421 and B17).

Figure 12 displays the relation between the orbital periods and eccentricities for eight of the systems in Cyg OB2 (open diamonds), six of the systems in NGC 6231 (solid triangles) and 66 of the systems in the 9th Spectroscopic Binary catalog (asterisks). The eccentricities in Cyg OB2 range from circular to moderately eccentric (0.291), while the total distribution in Figure 12 has an eccentricity range of zero to  $\sim 0.75$  for periods ranging from  $\sim 0.5$  days to 100 days. Systems with periods less than a few days tend toward more circular orbits, while systems with larger periods ( $> 10$  days) display a full range of eccentricities. This agrees

with previous studies such as Giuricin et al. (1984). There is a paucity of highly eccentric systems longer than 30 days. This likely stems from an incompleteness of the surveys at longer periods and is not a true trend. The Cyg OB2 star, A45, falls on the high-eccentricity side of the shorter period systems with an eccentricity of 0.273 and a period of 2.884 days. It does not appear to be particularly close to the majority of OB stars in the cluster center (see Figure 10), and so dynamical interaction with a massive neighbor does not seem a likely source of its higher eccentricity (unless it is a runaway system). It is possible that further observations of this system will constrain the eccentricity to a slightly more circular orbit, but its position in the figure is hardly removed from the rest, and therefore, its moderately elliptical orbit is not extraordinary. The remainder of Cyg OB2 stars fall well within the remaining distribution.

With the exception of MT421 and MT429, all the Cyg OB2 systems have early-type companions and mass ratios widely ranging from  $q \geq 0.19$  (MT258) to  $q = 0.99 \pm 0.02$  (Schulte 73). One may see this as an indication that the companions are not randomly drawn from a Salpeter (1955) or similar field star initial mass function (IMF). However, given that the current sample encompasses a number of systems that are double-lined spectroscopic binaries (i.e., they are easier to detect) this assessment may be premature and biased. Only time will tell, as we have a number of single-lined spectroscopic binary candidates still to investigate and a spectral database that has not been completely tapped. We continue to analyze these candidates with the long term goal of providing accurate distributions for binary orbital parameters of massive stars with an assumed shared formation history.

We thank the time allocation committees of the Lick, Keck, WIYN, and WIRO observatories for granting us observing time and making this project possible. We are also grateful for support from the National Science Foundation through Research Experience for Undergraduates (REU) program grant AST 03-53760 and through grant AST 03-07778, and the support of the Wyoming NASA Space Grant Consortium through grant NNG05G165H. We would also like to graciously thank, in no particular order, Christopher Rodgers, Emily May, Megan Bagley, Michael DiPompeo, Michael Alexander, Jessie Runnoe, and Sabrina Cales for their generous help in observing at WIRO through good skies and bad, and Jerry Bucher and James Weger for their ample help and upkeep of WIRO facilities.

*Facilities:* WIRO (), WIYN (), Lick (), Keck:I ()

## REFERENCES

Bonnell, I. A., Bate, M. R., & Zinnecker, H. 1998, MNRAS, 298, 93

- Comerón, F., et al. 2002, *A&A*, 389, 874
- Comerón, F., & Pasquali, A. 2007, *A&A*, 467, 23
- Conti, P. S, Leep, E. M. 1974, *ApJ*, 193, 113
- Contreras, M. E., Rodriguez, L. F., Tapia, M., Cardini, D., Emanuele, A., Badiali, M., & Persi, P. 1997, *ApJ*, 488, 153
- De Becker, M., Rauw, G., & Manfroid, J. 2004, *A&A*, 424, L39
- Drilling, J. S., & Landolt, A. U. 2000, in *Astrophysical Quantities*, ed. A. N. Cox (4th ed.; New York; Springer), 381
- Galazutdinov, G. A., Musaev, F. A., Krelowski, J., & Walker, G. A. H. 2000, *PASP*, 112, 648
- Giuricin, G., Mardirossian, F., & Mezzetti, M. 1984, *A&A*, 134, 365
- Hanson, M. M. 2003, *ApJ*, 597, 957
- Harmanec, P., Bisikalo, D. V., Boyarchuk, A. A., & Kuznetsov O. A. 2002, *A&A*, 396, 937
- Herbig, G. H. 1975, *ApJ*, 196, 129
- Herbig, G. H., & Leka, K. D. 1991, *ApJ*, 382, 193
- Hillwig, T. C., Gies, D. R., Bagnuolo, W. G., Jr., Huang, W., McSwain, M. V., & Wingert, D. W. 2006, *ApJ*, 639, 1069
- Kiminki, D. C., et al. 2007, *ApJ*, 664, 1120
- Kiminki, D. C., McSwain, M. V., & Kobulnicky, H. A. 2008, *ApJ*, 679, 1478
- Kinemuchi, K., et al. 2008, in prep
- Knödlseeder, J. 2000, *A&A*, 360, 539
- Kurtz, M. J., Mink, D. J., Wyatt, W. F., Fabricant, D. G., Torres, G., Kriss, G. A., & Tonry, J. L. 1991, in *Astronomical Data Analysis Software and Systems I*, ASP Conf. Ser., Vol. 25, eds. D.M. Worrall, C. Biemesderfer, and J. Barnes, p. 432
- Larson, R. B. 2001, *IAU Symposium*, 200, 93
- Lanz, T., & Hubeny, I. 2003, *ApJS*, 146, 417

- Linder, N., Rauw, G., Sana, H., De Becker, M., & Gosset, E. 2007, *A&A*, 474, 193
- Liu, Q.-Y.; Yang, Y.-L. 2003, *Chinese Journal of Astronomy and Astrophysics*, 3, 142
- Martins, F., Schaerer, D., & Hillier, D. J. 2005, *A&A*, 436, 1049
- Massey, P., & Thompson, A. B. 1991, *AJ*, 101, 1408
- Massey, P., Puls, J., Pauldrach, A. W. A., Bresolin, F., Kudritzki, R. P., & Simon, T. 2005, *ApJ*, 627, 477
- McSwain, M. V. 2003, *ApJ*, 595, 1124
- McSwain, M. V. 2007, *ApJ*, 655, 473
- Miczaika, G. R. 1953, *PASP*, 65, 141
- Milone, E. F. 1968, *AJ*, 73, 708
- Morbey, C. L., & Brosterhus, E. B. 1974, *PASP*, 86, 455
- Morton, D. C. 1991, *ApJ*, 77, 119
- Nazé, Y., De Becker, M., Rauw, G., & Barbieri, C. 2008, *A&A*, 483, 543
- Negueruela, I., Marco, A., Herrero, A., & Clark, J. S. 2008, *A&A*, 487, 575
- Öpik, E. J. 1924, *Tartu Obs. Publ.*, 25
- Otero, S. 2008a, *Open European Journal on Variable Stars*, 83, 1
- Otero, S. 2008b, *Open European Journal on Variable Stars*, 91, 1
- Penny, L. R., Ouzts, C., & Gies, D. R. 2008, 681, 554
- Pourbaix D., Tokovinin A. A., Batten A. H., Fekel F. C., Hartkopf W. I., Levato H., Morrell N. I., Torres G., Udry, S. 2004, *A&A*, 424, 727
- Pigulski, A., & Kolaczowski, Z. 1998, *MNRAS*, 298, 753
- Rauw, G., Vreux, J. M., & Bohannan, B. 1999, *ApJ* 517, 416
- Rios, L. Y., & DeGioia-Eastwood, K. 2004, *BAAS*, 205, No. 09.05
- Roberts, D. H., Lehár, J., & Dreher, J. W. 1987, *AJ*, 93, 968
- Romano, G. 1969, *MmSAI*, 40, 375

- Salpeter, E. E. 1955, *ApJ*, 121, 161
- Sana, H., Gosset, E., Nazé Y., Rauw, G., & Linder, N. 2008, *MNRAS*, 386, 447
- Schulte, D. H. 1956, *ApJ*, 123, 250
- Stefanik, R. P., Latham, D. W., Torres, G. 1999, *ASPC*, 185, 354
- Stroud, V. E., Clark, J.S., Negueruela, I. , Roche, P., & Norton, A.J. 2009, *A&A*, submitted
- Walborn, N. R. 1973, *ApJ*, 180, L35
- Walborn, N. R., & Fitzpatrick, E. L. 1990, *PASP*, 102, 379
- Walborn, N. R., & Howarth, I. D. 2000, *PASP*, 112, 1446
- Williams, et al. 2008, *ApJ*, 682, 492
- Wilson, O. C. 1948, *PASP*, 60, 385
- Wilson, O. C., & Abt, A. 1951, *ApJ*, 144, 477
- Wozniak, P. R., et al. 2004, *AJ*, 127, 2436, Northern Sky Variability Survey: Public Data Release

Table 1. Summary of Observing Runs

Date	Observatory/ Instrument	Spectral Coverage (Å)	Grating (1 mm <sup>-1</sup> )	Mean Spectral Resolution (Å)	Date Coverage (HJD)
1999 Jul 4–5	Keck/HIRES	3890–6270 in 35 orders	31.6	0.1	2,451,363–2,451,364
1999 Jul 21–23	Lick/Hamilton	3650–7675 in 81 orders	31.6	0.1	2,451,381–2,451,383
1999 Aug 21–23	Lick/Hamilton	3650–7675 in 81 orders	31.6	0.1	2,451,411–2,451,413
1999 Oct 14–15	Keck/HIRES	3700–5250 in 29 orders	31.6	0.1	2,451,466–2,451,467
2000 Jul 10–11	Lick/Hamilton	3650–7675 in 81 orders	31.6	0.1	2,451,736–2,451,737
2000 Sep 18–19	Keck/HIRES	3700–5250 in 29 orders	31.6	0.1	2,451,805–2,451,806
2001 Aug 24	WIYN/Hydra	3800–4490 in order 2	1200	0.9	2,452,146
2001 Sep 8–9	WIYN/Hydra	3800–4490 in order 2	1200	0.9	2,452,161–2,452,162
2004 Nov 28–30	WIYN/Hydra	3800–4490 in order 2	1200	0.9	2,453,338–2,453,340
2005 Jul 18–21	WIRO/WIRO-Spec	3800–4490 in order 1	2400	2.5	2,453,570–2,453,573
2005 Jul 18–20,22	WIRO/WIRO-Spec	3800–4490 in order 1	2400	2.5	2,453,632–2,453,635
2005 Oct 13	WIRO/Longslit	4050–6050 in order 2	600	2.5	2,453,657
2006 Jun 16–20	WIRO/Longslit	3900–5900 in order 2	600	2.5	2,453,903–2,453,907
2006 Jul 15–16,20	WIRO/Longslit	3900–5900 in order 2	600	2.5	2,453,932–2,453,935
2006 Sep 8–11	WIYN/Hydra	3800–4490 in order 2	1200	0.9	2,453,987–2,453,990
2006 Oct 7	WIRO/Longslit	3900–5900 in order 2	600	2.5	2,454,016
2007 Jun 28–30	WIRO/Longslit	3900–5900 in order 2	600	2.5	2,454,280–2,454,282
2007 Jul 4–6	WIYN/Hydra	3820–4510 in order 2	1200	0.9	2,454,285–2,454,287
2007 Aug 28–Sep 4	WIRO/Longslit	5550–6850 in order 1	1800	1.5	2,454,341–2,454,348
2007 Oct 23,25,27–29,31	WIRO/Longslit	5550–6850 in order 1	1800	1.5	2,454,397–2,454,405
2007 Nov 1,3–5	WIRO/Longslit	5550–6850 in order 1	1800	1.5	2,454,406–2,454,410
2008 Jun 10–15	WIYN/Hydra	3820–4510 in order 2	1200	0.9	2,454,628–2,454,633
2008 Jun 23–30	WIRO/Longslit	5210–6680 in order 1	1800	1.5	2,454,641–2,454,648
2008 Jul 21,22–27	WIRO/Longslit	5250–6740 in order 1	1800	1.5	2,454,669–2,454,675
2008 Aug 17–22	WIRO/Longslit	5250–6740 in order 1	1800	1.5	2,454,696–2,454,701
2008 Sep 12,13–16,19	WIRO/Longslit	5250–6740 in order 1	1800	1.5	2,454,722–2,454,729
2008 Oct 14–18	WIRO/Longslit	5250–6740 in order 1	1800	1.5	2,454,754–2,454,758

Table 2. Orbital Elements

Element	MT145	A36	A45	Schulte 73	MT372
$P$ (Days)	25.140 (0.008)	4.674 (0.004)	2.884 (0.001)	17.28 (0.03)	2.228 (fixed)
$e$	0.291 (0.009)	0.10 (0.01)	0.273 (0.002)	0.169 (0.009)	0.0 (fixed)
$\omega$ (deg)	158.3 (0.6)	359.2 (0.7)	188.8 (0.1)	7.3 (0.8)	344 (146)
$\gamma$ (km s <sup>-1</sup> )	-19.3 (0.4)	-47 (2)	5 (1)	-11 (2)	3 (7)
$T_0$ (HJD-2,400,000)	51789.08 (0.04)	54693.836 (0.009)	54728.209 (0.001)	54700.89 (0.03)	54755 (9)
$K_1$ (km s <sup>-1</sup> )	48.9 (0.7)	169 (9)	126.1 (0.3)	117 (2)	75 (20)
$K_2$ (km s <sup>-1</sup> )	...	243 (2)	273 (17)	117.9 (0.8)	...
$M_1$ (M <sub>⊙</sub> )	22.6 (0.5) <sup>a</sup>	>19.8 (0.9) <sup>c</sup>	>12 (1) <sup>c</sup>	>11.2 (0.2) <sup>c</sup>	17.5 <sup>b</sup>
$M_2$ (M <sub>⊙</sub> )	6.0 (0.1)–13.8 (0.6)	>13.8 (0.9) <sup>c</sup>	>5.3 (0.5) <sup>c</sup>	>11.1 (0.2) <sup>c</sup>	~10.0 <sup>b</sup>
$f(m)_1$ (M <sub>⊙</sub> )	0.267 (0.012)	6.9 (0.2)	0.534 (0.004)	2.8 (0.1)	0.099 (0.080)
$f(m)_2$ (M <sub>⊙</sub> )	...	2.3 (0.4)	5 (1)	2.81 (0.06)	...
S. C. <sub>1</sub>	O9III	B0Ib	B0.5V	O8III	B0V
S. C. <sub>2</sub>	mid B	B0III	B2V?–B3V?	O8III	B2?V
$a_1 \sin i$ (R <sub>⊙</sub> )	23.2 (0.3)	15.6 (0.8)	6.91 (0.02)	39.4 (0.5)	3.4 (0.9)
$a_2 \sin i$ (R <sub>⊙</sub> )	...	22.345 (0.003)	14.96 (0.01)	39.675 (0.004)	...
$rms_1$ (km s <sup>-1</sup> )	8.9	29.3	25	5.1	14.9
$rms_2$ (km s <sup>-1</sup> )	...	10.0	47	6.7	...

Note. — Calculated errors are located in parentheses.

<sup>a</sup>Theoretical O star masses adopted from Martins et al. (2005).

<sup>b</sup>Theoretical B star masses interpolated from Drilling & Landolt (2000).

<sup>c</sup>Calculated mass is equal to  $M \sin^3 i$ .

Table 3. Ephemerides for MT145 & MT372

Date (HJD-2,400,000)	$\phi$	$V_r$ (km s <sup>-1</sup> )	1 $\sigma$ err (km s <sup>-1</sup> )	$O - C$ (km s <sup>-1</sup> )
51,381.50.....	0.788	1.7	10.3	1.8
51,383.50.....	0.867	-24.7	15.1	-1.0
51,467.90.....	0.225	-21.5	4.4	9.2
51,736.50.....	0.909	-33.5	11.3	7.8
51,737.50.....	0.948	-56.4	13.7	3.5
51,805.76.....	0.664	22.8	3.2	7.9
52,146.70.....	0.225	-23.6	3.6	6.9
52,161.81.....	0.826	-7.4	4.1	2.4
52,162.67.....	0.860	-17.8	3.8	3.3
53,338.63.....	0.637	14.0	4.4	-1.9
53,340.59.....	0.715	10.7	4.2	-0.4
53,570.50.....	0.860	-40.0	8.3	-18.9
53,572.50.....	0.940	-66.4	10.0	-10.3
53,632.50.....	0.327	-10.5	11.5	-2.7
53,633.50.....	0.367	-10.6	6.7	-9.3
53,636.50.....	0.486	11.5	5.2	-0.3
53,657.50.....	0.321	-0.8	6.8	8.0
53,903.75.....	0.116	-71.7	8.4	-7.1
53,903.76.....	0.117	-74.7	9.1	-10.3
53,904.72.....	0.155	-33.1	7.8	18.8
53,904.73.....	0.155	-41.0	7.6	10.7
53,904.90.....	0.162	-65.6	7.7	-16.1
53,905.77.....	0.197	-49.4	6.8	-10.6
53,905.90.....	0.202	-48.1	7.3	-11.0
53,906.74.....	0.235	-19.3	8.5	8.6
53,906.89.....	0.241	-42.2	10.6	-15.8
53,907.78.....	0.277	-20.5	10.2	-2.7
53,907.88.....	0.280	-28.4	7.1	-11.4
53,932.75.....	0.270	-17.0	7.9	2.5
53,932.85.....	0.274	2.5	8.8	20.9
53,932.86.....	0.274	6.4	10.3	24.8
53,935.89.....	0.395	-14.7	12.8	-17.3
53,987.70.....	0.456	1.8	4.6	-7.6
53,988.75.....	0.497	9.9	4.4	-2.8
53,989.66.....	0.534	13.7	4.7	-1.0
53,990.86.....	0.581	17.3	4.3	1.1
54,280.83.....	0.116	-61.7	7.0	3.0
54,280.87.....	0.117	-56.5	6.6	7.8
54,281.70.....	0.150	-60.2	8.5	-6.7
54,281.78.....	0.153	-50.9	7.8	1.4
54,281.85.....	0.156	-51.5	7.0	-0.0
54,282.70.....	0.190	-44.8	7.9	-4.1
54,282.77.....	0.193	-45.6	6.0	-5.7
54,282.83.....	0.195	-45.9	6.9	-6.8
54,285.93.....	0.318	-6.0	4.3	3.3

Table 3—Continued

Date (HJD-2,400,000)	$\phi$	$V_r$ (km s <sup>-1</sup> )	1 $\sigma$ err (km s <sup>-1</sup> )	$O - C$ (km s <sup>-1</sup> )
54,286.66.....	0.348	-7.6	5.2	-3.4
54,287.73.....	0.390	5.3	4.3	3.2
54,397.71.....	0.765	5.0	16.7	0.7
54,399.69.....	0.843	-22.0	15.3	-6.9
54,401.67.....	0.922	-47.9	16.0	-0.3
54,402.71.....	0.964	-54.1	14.6	12.3
MT372				
54,754.62.....	0.949	75.4	7.4	9.8
54,755.60.....	0.388	-36.6	6.3	1.7
54,756.60.....	0.840	16.0	3.0	-8.9
54,757.59.....	0.283	6.9	3.9	-1.9
54,758.72.....	0.788	6.9	3.4	6.3

Table 4. Ephemerides for A36, A45, & Schulte 73

Date (HJD-2,400,000)	$\phi$	$V_{r1}$ (km s <sup>-1</sup> )	$O_1 - C_1$ (km s <sup>-1</sup> )	$V_{r2}$ (km s <sup>-1</sup> )	$O_2 - C_2$ (km s <sup>-1</sup> )
A36					
54,403.61.....	0.910	-163.4 (5.6)	27.7	167.5 (4.9)	4.2
54,403.70.....	0.928	-174.9 (5.0)	30.9	184.7 (4.3)	1.0
54,405.71.....	0.357	103.4 (5.3)	47.6	-194.2 (3.5)	3.1
54,406.63.....	0.555	105.4 (3.7)	5.6	-261.1 (3.4)	-5.3
54,406.76.....	0.582	108.6 (3.7)	16.2	-244.5 (3.7)	0.2
54,409.73.....	0.218	-23.6 (5.5)	45.3	-23.0 (3.7)	-3.3
54,410.67.....	0.419	98.4 (3.7)	10.5	-243.8 (3.4)	-1.8
54,628.88.....	0.103	-163.3 (2.6)	24.6	147.2 (2.5)	-5.3
54,633.74.....	0.143	-150.6 (3.1)	-0.8	108.1 (3.3)	11.0
54,669.84.....	0.867	-116.5 (6.2)	34.0	113.4 (4.1)	7.4
54,672.78.....	0.495	100.3 (3.8)	-4.4	-280.6 (3.7)	-16.1
54,673.88.....	0.730	-37.7 (12.9)	-33.6	-92.2 (7.1)	11.6
54,696.69.....	0.610	109.0 (14.4)	27.6	-236.8 (3.5)	-8.4
54,696.96.....	0.669	125.2 (4.3)	79.0	-155.7 (3.9)	21.1
54,697.66.....	0.818	-129.9 (5.9)	-32.7	23.1 (3.4)	-6.8
54,697.96.....	0.882	-163.1 (4.3)	2.4	129.6 (3.7)	2.4
54,698.75.....	0.052	-198.2 (4.4)	24.4	200.8 (7.1)	-2.9
54,700.87.....	0.505	103.7 (3.7)	-1.3	-254.3 (3.4)	10.3
54,701.90.....	0.724	1.7 (3.6)	0.8	-114.0 (3.8)	-2.9
A45					
54,403.66.....	0.447	106.3 (14.89)	-6.7	-257.5 (5.33)	-28.2
54,403.74.....	0.476	127.4 (12.48)	14.6	-225.1 (6.17)	3.9
54,405.72.....	0.161	7.9 (5.40)	3.8	-33.0 (25.14)	-39.6
54,405.74.....	0.169	-56.9 (6.78)	-67.9	-12.9 (16.19)	-4.5
54,406.64.....	0.483	87.3 (15.39)	-25.3	-200.5 (8.72)	28.0
54,406.65.....	0.486	87.3 (20.36)	-25.1	-165.5 (11.95)	62.6
54,406.77.....	0.527	135.4 (13.52)	26.4	-171.1 (7.89)	49.6
54,409.74.....	0.557	126.6 (9.00)	21.8	-226.0 (5.93)	-14.5
54,410.68.....	0.882	-84.1 (14.51)	-9.6	233.8 (6.10)	57.1
54,641.84.....	0.046	-126.0 (5.87)	-14.6	226.6 (6.80)	-30.0
54,647.81.....	0.116	-28.5 (8.80)	11.4	4.0 (8.07)	-97.9
54,672.90.....	0.817	9.7 (15.16)	26.3	8.3 (19.51)	-43.0
54,724.70.....	0.784	-17.0 (17.09)	-26.4	4.0 (23.56)	9.0
54,724.78.....	0.810	23.8 (7.31)	34.1	-1.4 (23.90)	-39.0
54,725.72.....	0.135	-17.0 (10.74)	3.9	6.8 (8.43)	-53.8
54,726.72.....	0.483	115.3 (10.66)	2.7	-250.6 (7.71)	-22.2
54,726.79.....	0.508	111.6 (13.80)	0.6	-228.2 (6.83)	-3.2
54,729.70.....	0.517	139.9 (11.19)	29.8	-234.4 (6.08)	-11.2
54,747.59.....	0.721	21.5 (5.86)	-27.6	-4.1 (6.10)	87.0
54,748.60.....	0.071	-76.2 (6.34)	11.4	285.4 (26.42)	80.1

Table 4—Continued

Date (HJD-2,400,000)	$\phi$	$V_{r1}$ (km s <sup>-1</sup> )	$O_1 - C_1$ (km s <sup>-1</sup> )	$V_{r2}$ (km s <sup>-1</sup> )	$O_2 - C_2$ (km s <sup>-1</sup> )
54,754.77.....	0.212	-15.6 (10.59)	-59.0	3.2 (44.57)	81.7
Schulte 73					
52,161.65.....	0.071	-133.5 (2.0)	-1.9	110.7 (2.0)	1.5
54,628.75.....	0.825	-118.3 (2.9)	-43.6	86.5 (2.5)	31.3
54,628.88.....	0.833	-112.4 (3.6)	-31.8	89.1 (2.1)	27.9
54,629.87.....	0.890	-157.5 (3.1)	-34.0	88.6 (2.1)	-15.3
54,630.74.....	0.941	-156.9 (2.9)	-4.9	121.3 (2.1)	-10.5
54,630.85.....	0.947	-166.7 (2.5)	-12.3	122.3 (2.1)	-11.9
54,633.86.....	0.121	-115.2 (2.4)	-22.0	95.6 (2.1)	25.5
54,696.75.....	0.760	-31.4 (6.8)	-5.4	0.5 (2.0)	-5.7
54,696.96.....	0.772	-13.4 (2.9)	21.2	16.1 (3.8)	1.1
54,697.77.....	0.819	-67.9 (5.3)	1.9	46.8 (1.8)	-3.5
54,697.85.....	0.824	-81.4 (3.0)	-8.0	60.9 (2.0)	6.9
54,697.92.....	0.828	-70.8 (2.9)	5.9	69.9 (2.4)	12.7
54,698.71.....	0.874	-122.4 (1.9)	-10.5	88.7 (1.8)	-3.7
54,698.91.....	0.885	-125.2 (3.1)	-5.0	107.1 (2.8)	6.5
54,699.72.....	0.932	-148.7 (1.4)	-0.6	127.3 (1.4)	-0.8
54,699.93.....	0.944	-142.4 (1.7)	10.9	138.2 (1.6)	5.1
54,700.72.....	0.990	-150.0 (2.1)	11.8	131.3 (1.6)	-9.5
54,701.73.....	0.048	-155.0 (1.8)	-9.8	126.9 (1.5)	3.7
54,701.94.....	0.061	-142.0 (2.7)	-3.8	124.4 (2.2)	8.4
54,724.69.....	0.377	66.8 (3.3)	6.6	-91.7 (2.8)	-8.2
54,724.81.....	0.384	73.1 (1.8)	11.2	-88.7 (1.4)	-3.6
54,725.69.....	0.435	69.4 (1.5)	-1.0	-93.3 (1.4)	-0.1
54,725.80.....	0.441	70.8 (1.6)	-0.2	-93.3 (1.5)	0.4
54,726.70.....	0.493	69.0 (1.7)	-3.0	-90.4 (1.6)	3.9
54,726.82.....	0.500	67.5 (1.6)	-4.2	-87.9 (1.5)	5.9
54,729.66.....	0.664	27.0 (2.0)	-2.4	-52.7 (1.9)	-2.8
54,729.84.....	0.675	22.2 (2.1)	-2.2	-52.9 (2.1)	-8.1

Table 5. OB Binaries in Cyg OB2

Star	Type	S.C.	P (days)	q	Ref.
MT059	SB1	O8V & B	4.8527 (0.0002)	0.22–0.67 <sup>a</sup>	1
MT145	SB1	O9III & mid B	25.140 (0.008)	0.26–0.63 <sup>a</sup>	2
MT252	SB2	B2III & B1V	18–19	0.8 (0.2)	1
MT258	SB1	O8V & B	14.660 (0.002)	0.18–0.89 <sup>a</sup>	1
MT372	EA?/SB1	B0V & B2?V	2.228 (fixed)	~0.6	2,3
MT421	EA	O9V & B9V–A0V	4.161	~0.16–0.19	4
MT429	EA	B0V & ??	2.9788	...	4
MT696	SB2/EW/KE	O9.5V & early B	1.46	...	5
MT720	SB2	early B & early B	< 5	...	1
MT771	SB2	O7V & O9V	1.5:	0.8 (0.1)	1
Schulte 3	SB2/EA?	O6IV? & O9III	4.7464 (0.0002)	0.44 (0.08)	1,6
Schulte 5	EB	O7Ianf & Ofpe/WN9 (& B0V?)	6.6	0.28 (0.02)	7,8,9,10,11,12
Schulte 8a	SB2	O5.5I & O6?	21.908	0.86 (0.04)	13,14
Schulte 9	SB2	O5? & O6–7?	2.355 yr	...	15
Schulte 73	SB2	O8III & O8III	17.28 (0.03)	0.99 (0.02)	2
A36	SB2/EA	B0Ib & B0III	4.674 (0.004)	0.70 (0.06)	2,16,17
A45	SB2	B0.5V & B2V?–B3V?	2.884 (0.001)	0.46 (0.02)	2,17
B17	SB2	O7? & O9?	4.0217 (0.0004)	~1?	18,19

Note. — Photometric types EW/KE, EA, and EB stand for Contact system of the W UMa type (ellipsoidal;  $P < 1$  day), Algol type (near spherical), and  $\beta$  Lyr type (ellipsoidal;  $P > 1$  day) respectively. The mass ratio for MT421 is calculated using the O star masses of Martins et al. (2005) and interpolated AB masses of Drilling & Landolt (2000). The mass ratio for Schulte 10 is calculated using the interpolated B star masses from Drilling & Landolt (2000).

<sup>a</sup>The range in mass ratio incorporates both observational and inclination uncertainties

References. — (1) Kiminki et al. (2008) (2) This work; (3) Wozniak et al. (2004); (4) Pigulski & Kolaczowski (1998); (5) Rios & DeGioia-Eastwood (2004); (6) Kinemuchi et al. (2008, in prep); (7) Wilson (1948); (8) Wilson & Abt (1951); (9) Miczaika (1953); (10) Walborn (1973); (11) Contreras et al. (1997); (12) Rauw et al. (1999); (13) Romano (1969); (14) De Becker et al. (2004); (15) Nazé et al. (2008); (16) Otero (2008a); (17) Hanson (2003); (18) Stroud et al. (2009, submitted); (19) Otero (2008b)

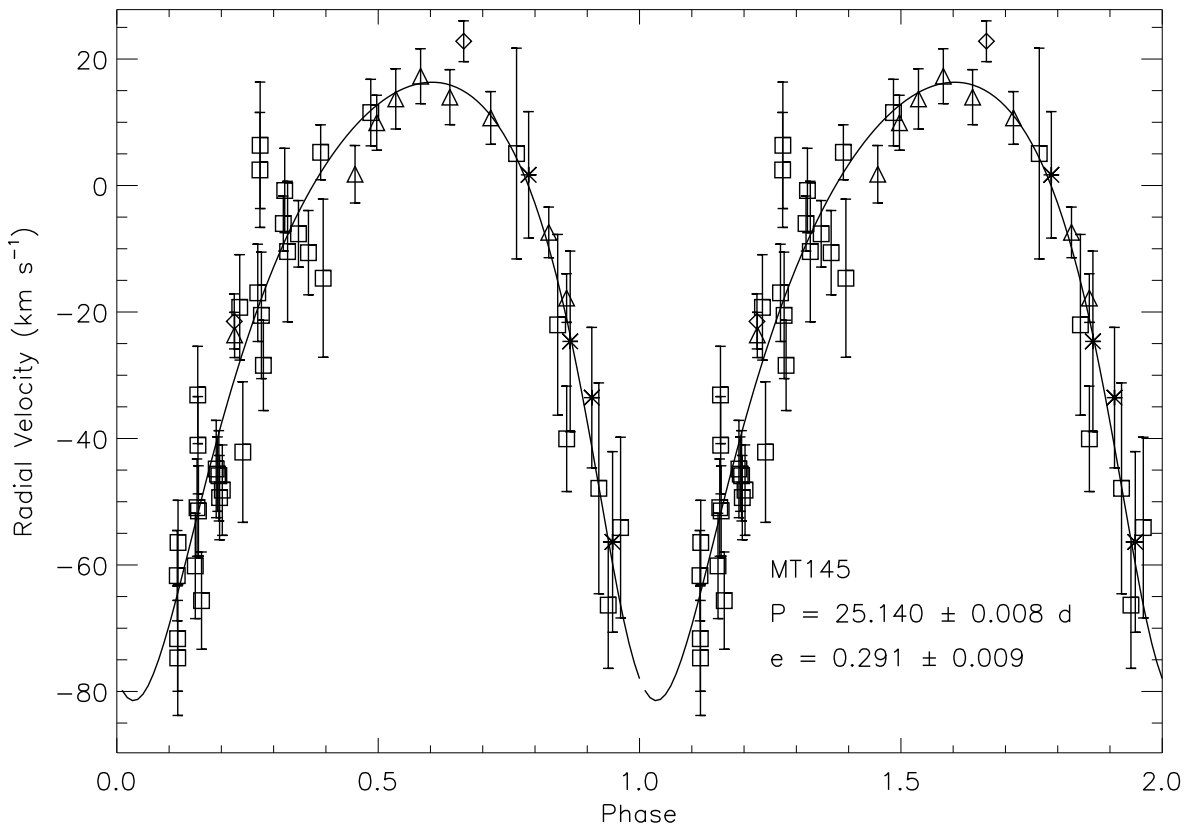


Fig. 1.—  $V_r$  curve and orbital solution to the O9III star, MT145. The symbols correspond to the different observatories, where the asterisks are observations taken with the Hamilton Spectrograph (Lick), the diamonds are observations taken with HIRES (Keck), the triangles are observations taken with Hydra (WIYN), and the squares are observations taken with WIROspec or the WIRO-Longslit Spectrograph.

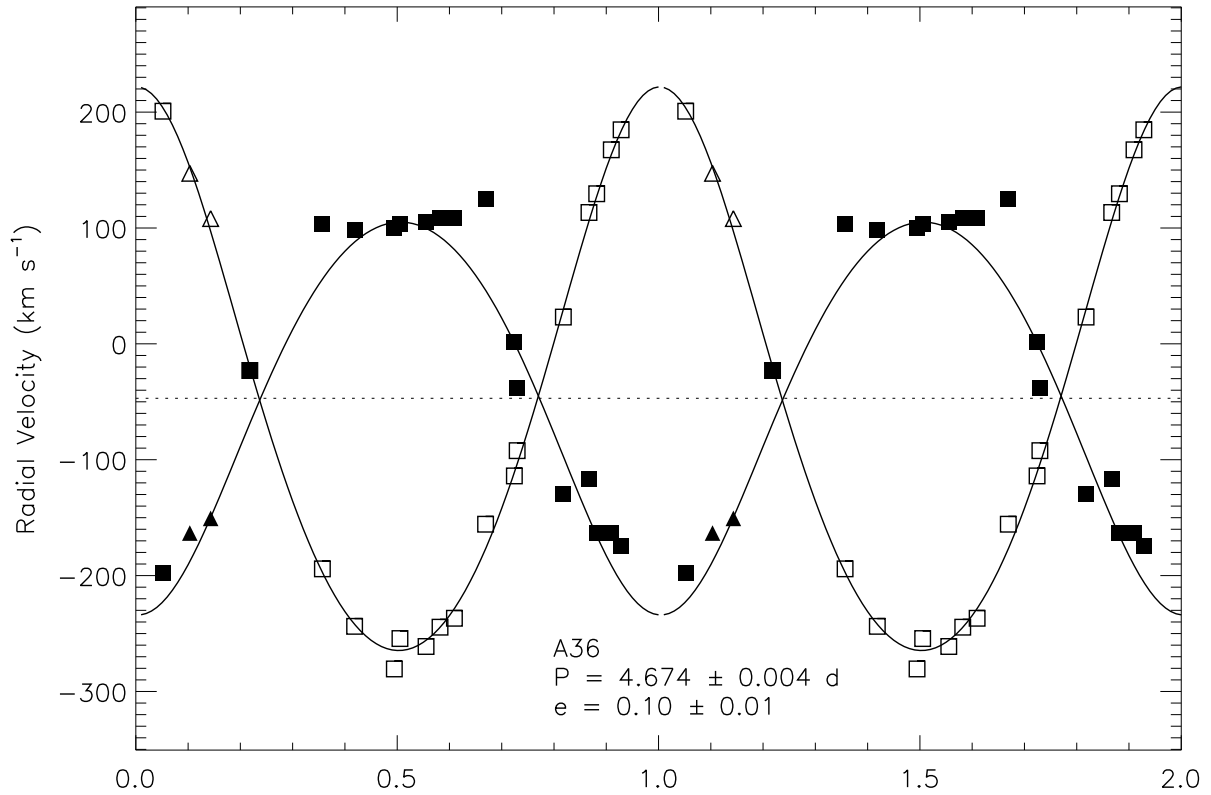


Fig. 2.—  $V_r$  curve and orbital solution for A36 using 19 of the 23 observations. The filled points correspond to the primary (B0Ib) and the open points correspond to the secondary (B0III). The symbols represent the same observation locations as in Figure 1.

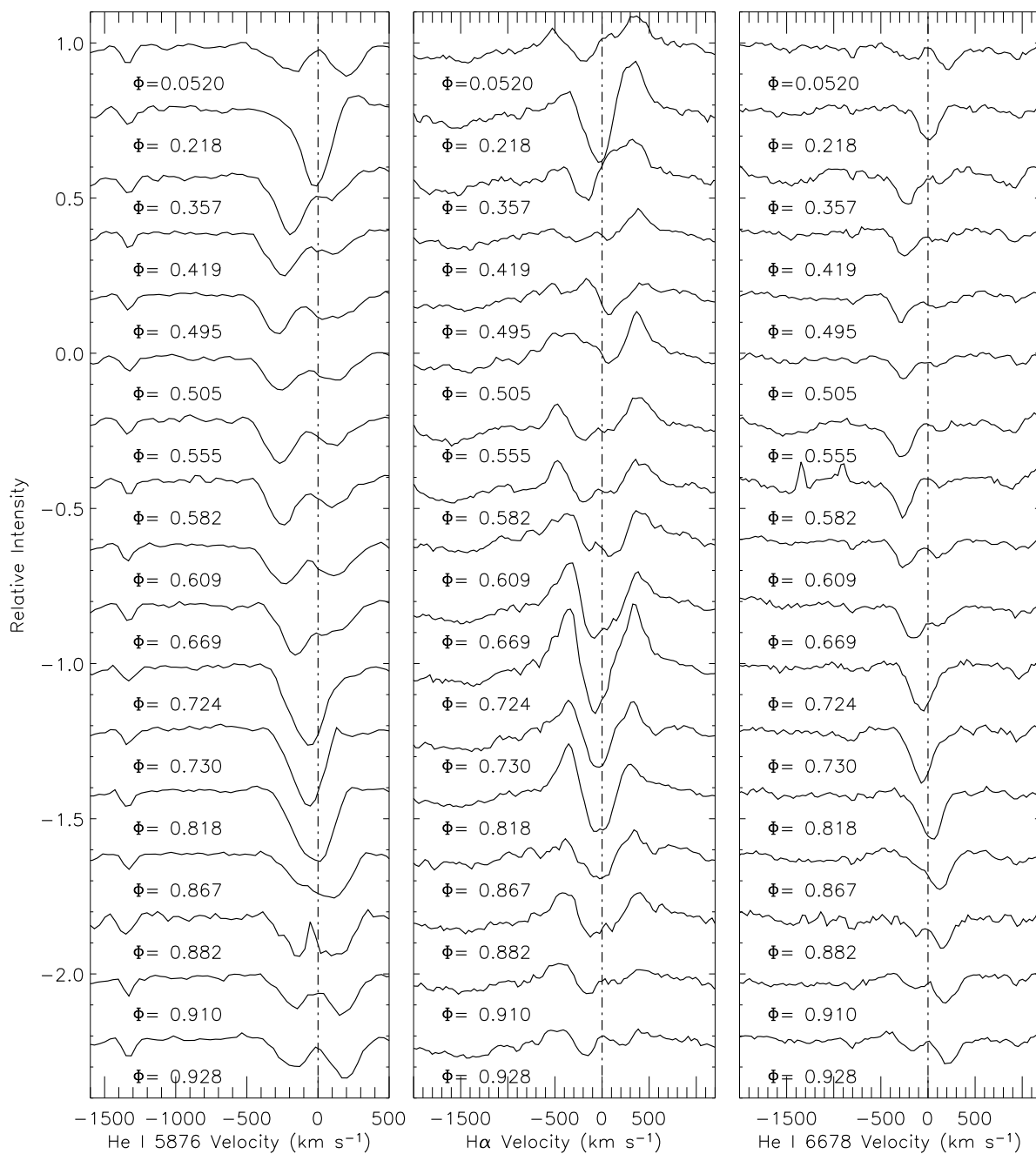


Fig. 3.— He I  $\lambda 5875.75$  (left), H $\alpha$   $\lambda 6562.80$  (middle), He I  $\lambda 6678.15$  (right) in velocity space and in order of phase for observations of A36 taken at WIRO between 2007 October and 2008 August.

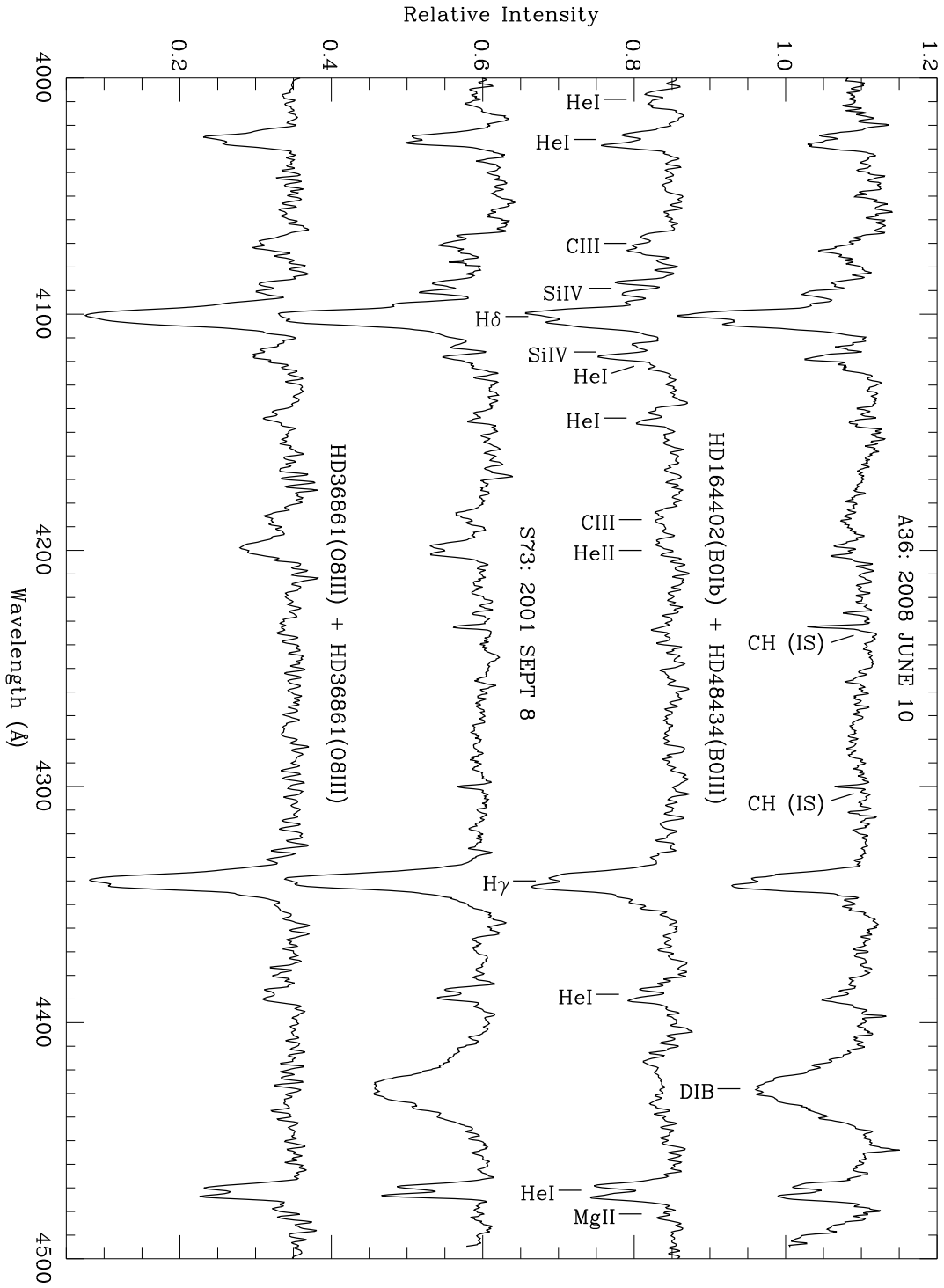


Fig. 4.— Spectra of A36 (*first*) and Schulte 73 (*third*) obtained with WIYN on 2008 June 10 and 2001 September 8 respectively and composites of two spectra from the Walborn & Fitzpatrick (1990) digital atlas shifted to the appropriate radial velocities (*second and fourth*) that best match the spectral types of the primaries and secondaries of A36 and Schulte 73. Absorption features are labeled at their respective intrinsic values.

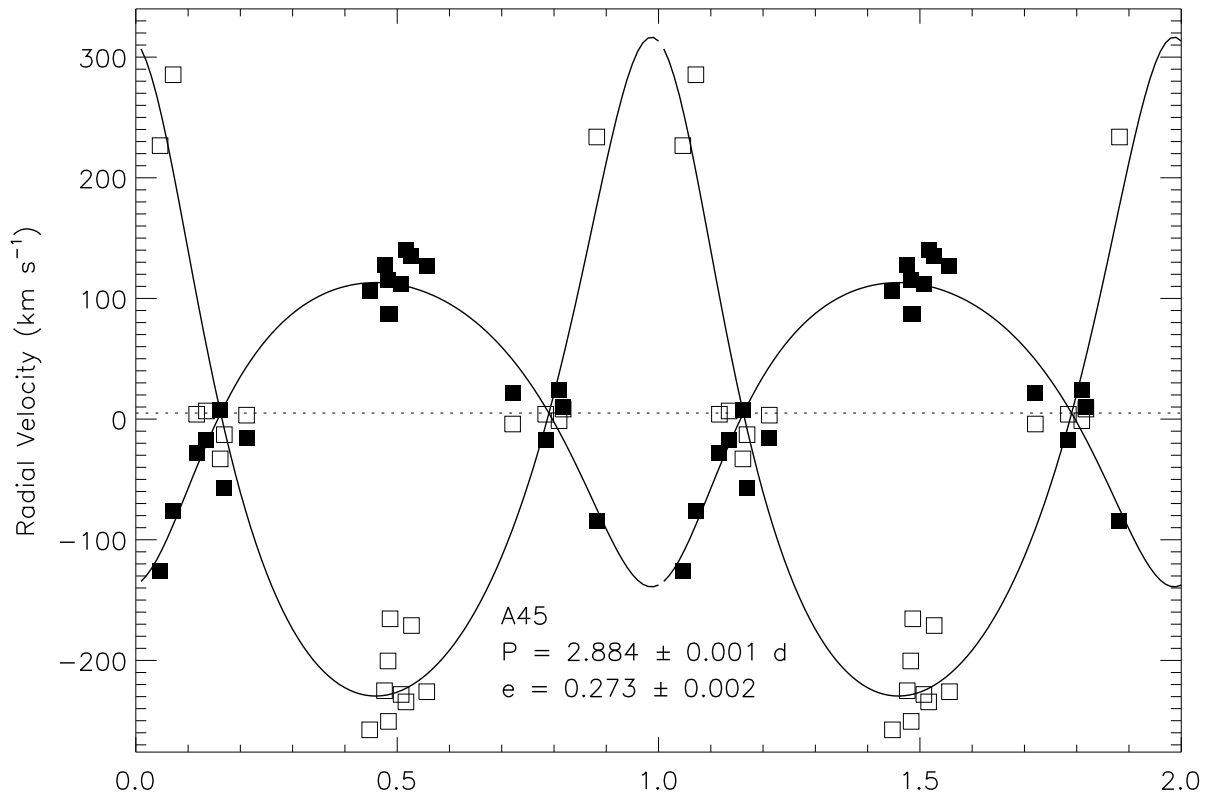


Fig. 5.—  $V_r$  curve and orbital solution for A45 using 21 of the 24 observations. The filled points correspond to the primary (B0.5V) and the open points correspond to the secondary (B2V?–B3V?). All data were obtained with the WIRO-Longslit spectrograph.

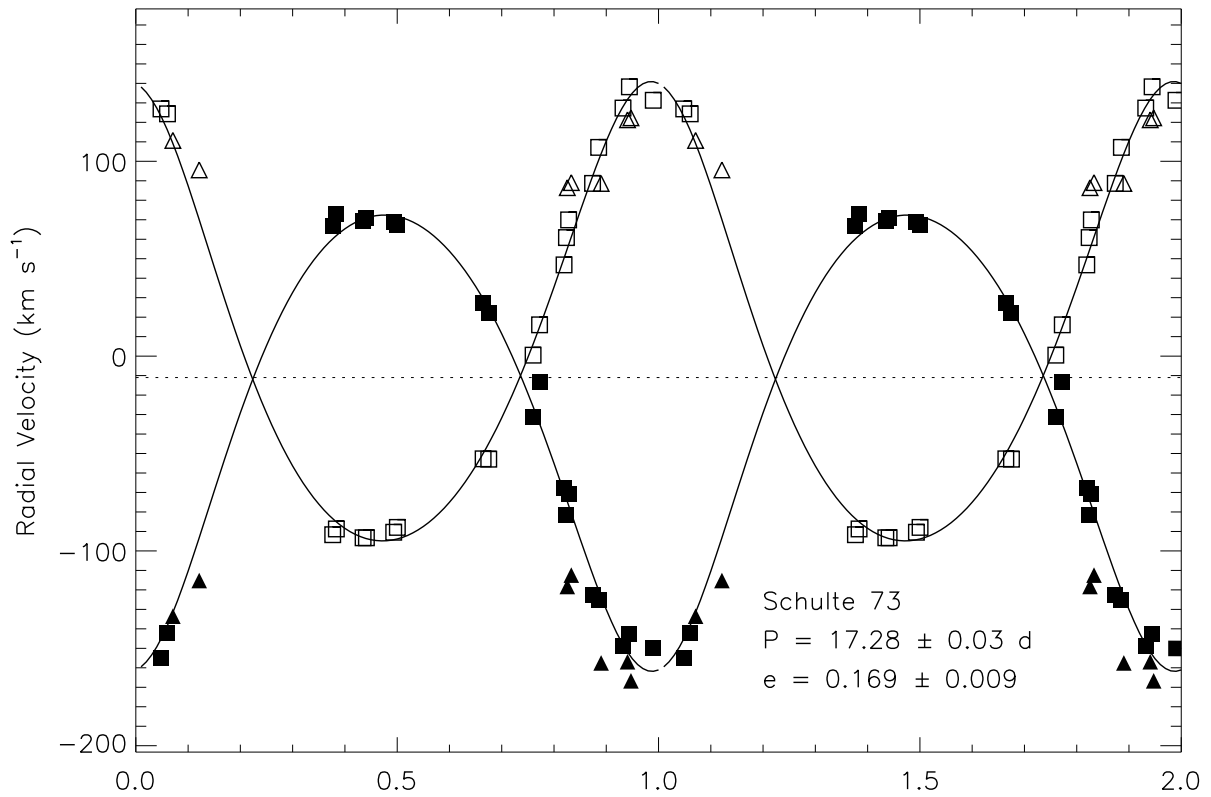


Fig. 6.—  $V_r$  curve and orbital solution for S73 using 27 of the 36 observations. The filled points correspond to the primary (O8III) and the open points correspond to the secondary (O8III). The symbols represent the same observation locations as in Figure 1.

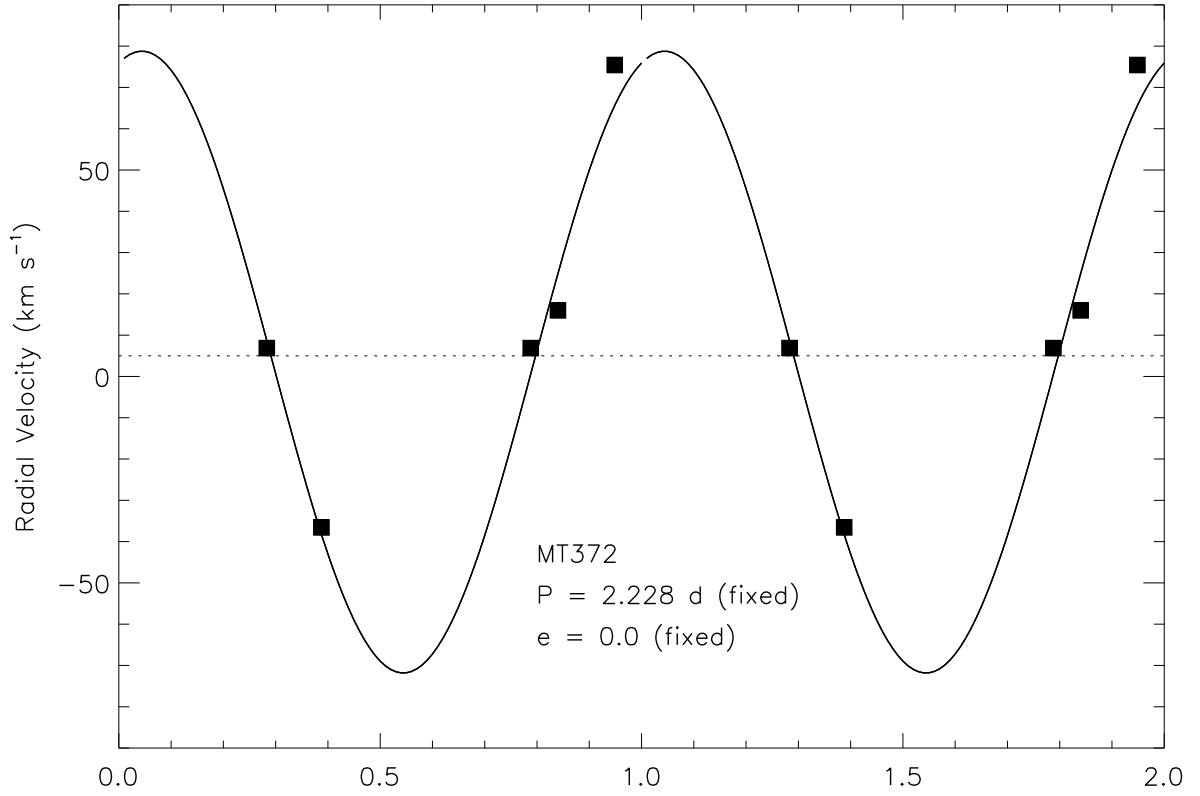


Fig. 7.—  $V_r$  curve and orbital solution for MT372 using 5 H $\alpha$  observations and the period obtained from the photometric data. All data were obtained with the WIRO-Longslit spectrograph.

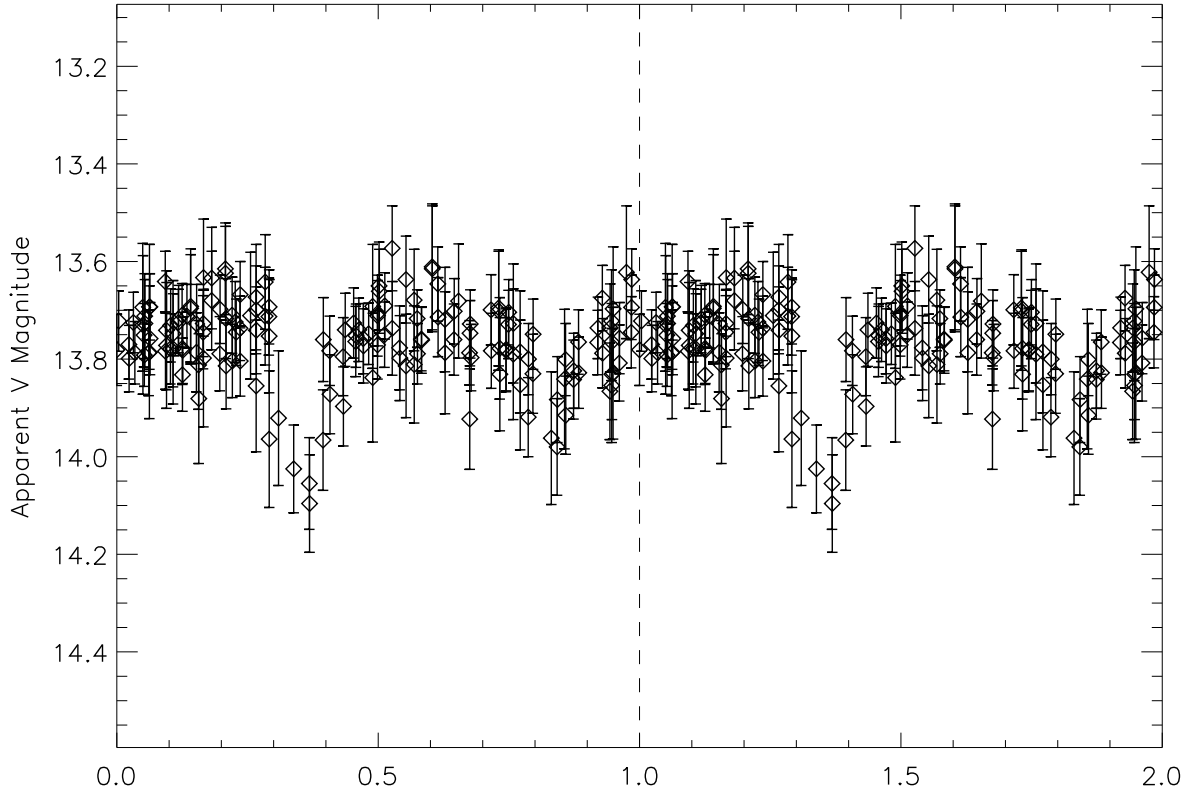


Fig. 8.— Folded light curve of MT372 ( $P = 2.228$  d) utilizing photometric data from the Northern Sky Variability Survey (Wozniak et al. 2004).

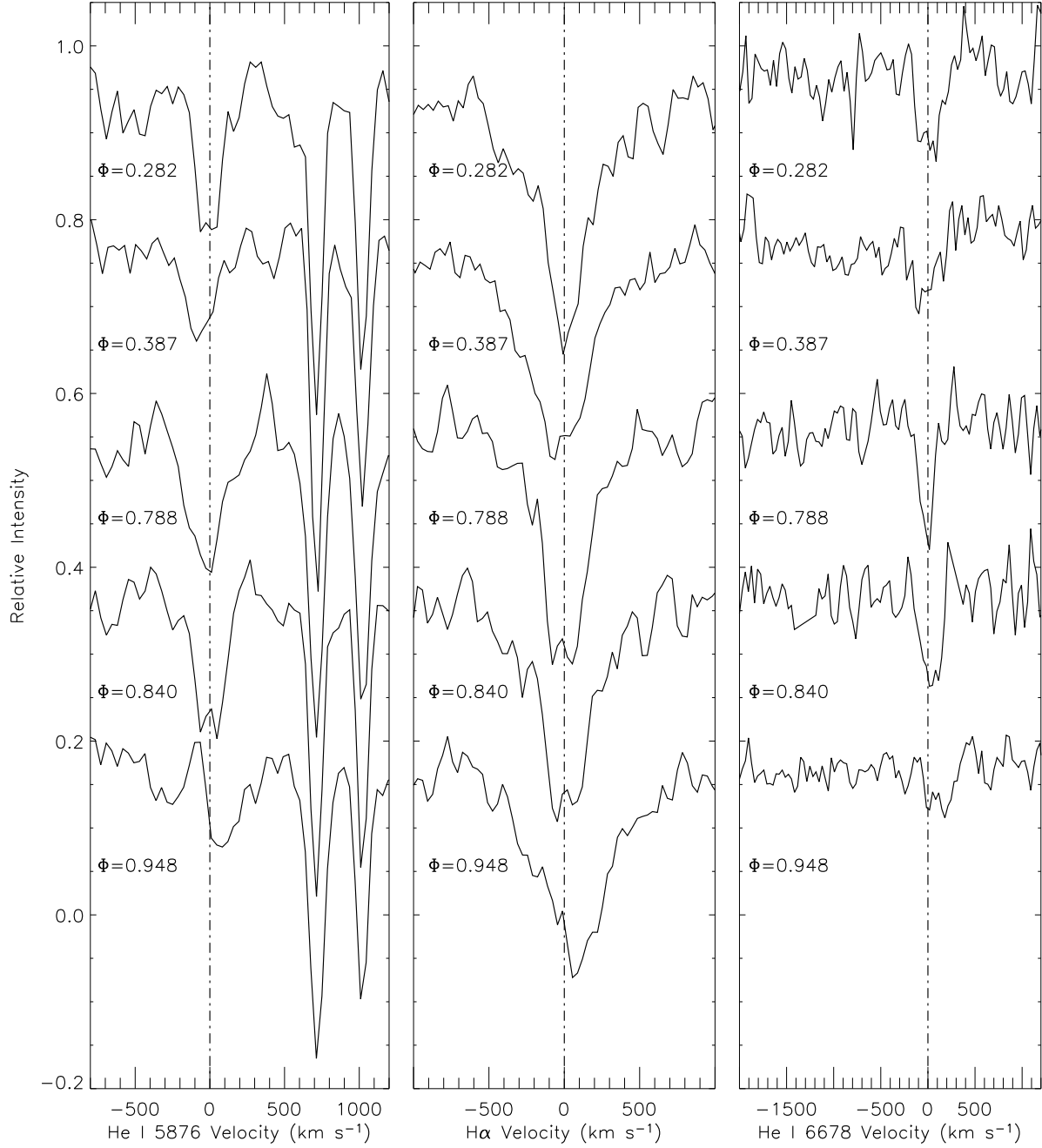


Fig. 9.— He I  $\lambda 5875.75$  (left), H $\alpha$   $\lambda 6562.80$  (middle), He I  $\lambda 6678.15$  (right) in velocity space and in order of phase for observations of MT372 taken at WIRO 2008 October 14–18.

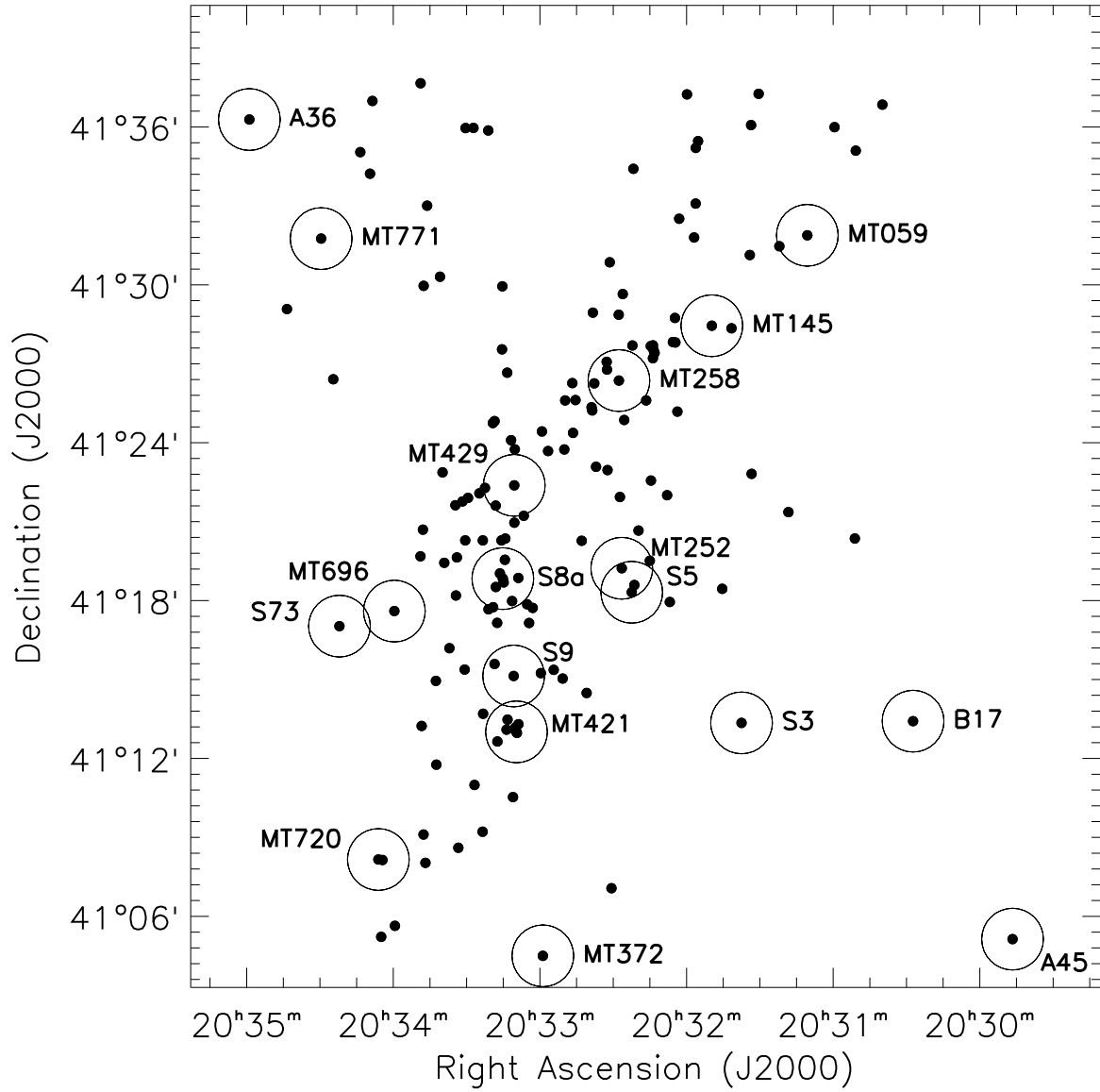


Fig. 10.— A map of OB stars in Cyg OB2. Circles indicate the locations of the 18 known binaries within Cyg OB2.

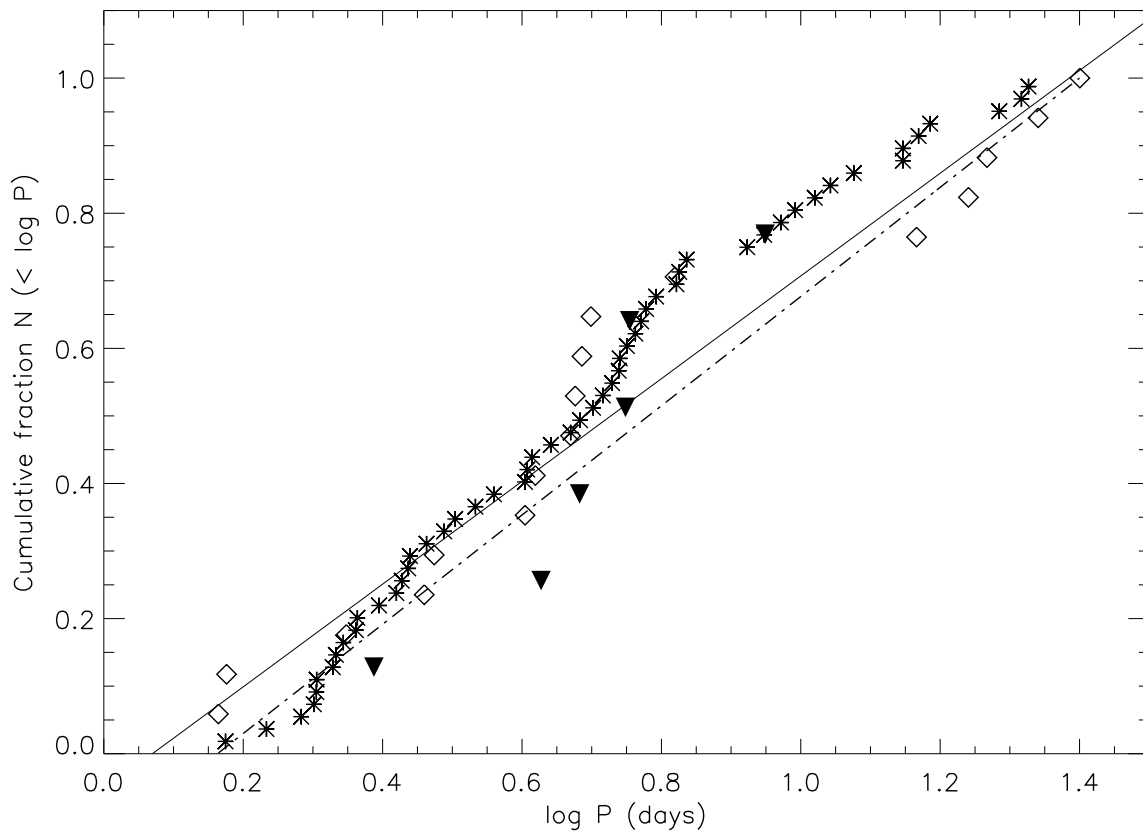


Fig. 11.— Cumulative fractions of the number of binary systems with periods less than 25.2 days in Cyg OB2 (open diamonds), NGC 6231 (solid triangles), and the OB stars from the 9th Spectroscopic Binary catalog (Pourbaix et al. 2004, asterisks), as a function of the logarithm of the period. The solid line represents the best linear fit to the Cyg OB2 distribution and is included for illustrative purposes. The dashed line represents a perfect Öpik distribution (i.e., the distribution of  $\log(P)$  is flat; Öpik 1924).

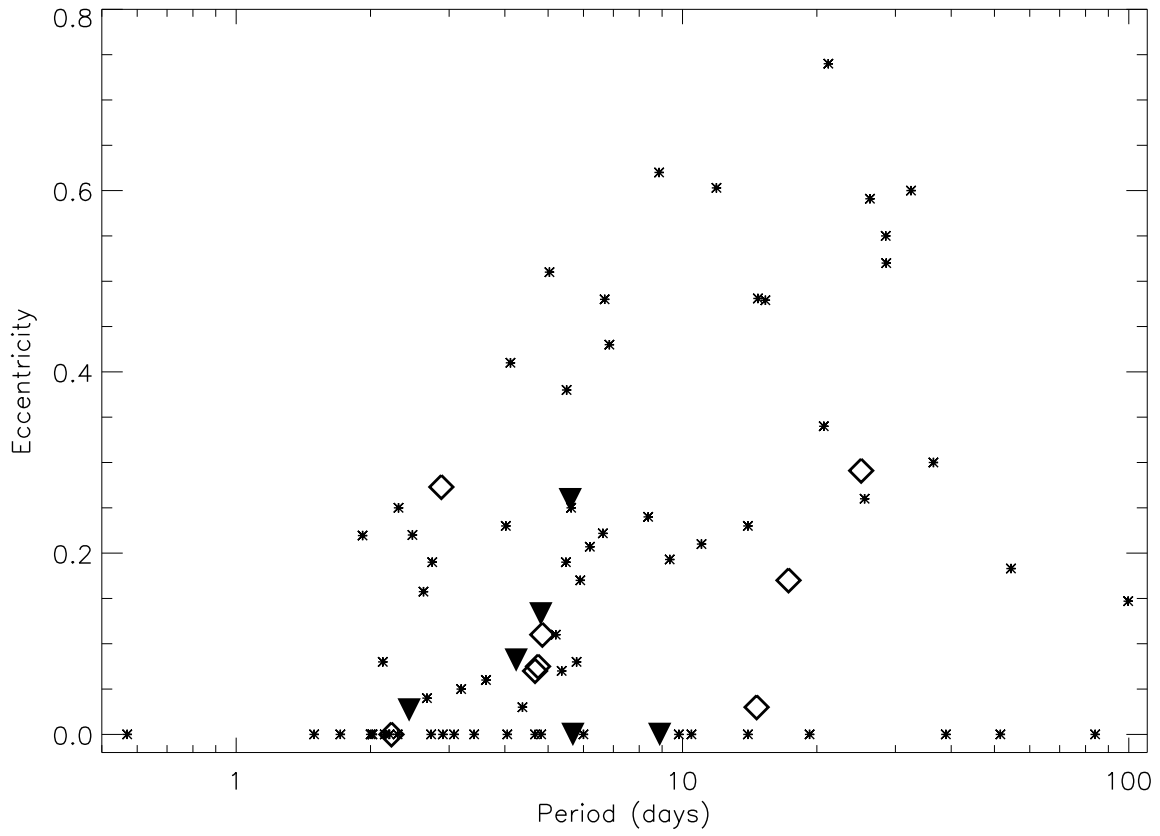


Fig. 12.— Period versus eccentricity for stars in Cyg OB2 (open diamonds), NGC 6231 (solid triangles) and the OB stars in the 9th Spectroscopic Binary catalog (asterisks).